Chapter 5: Characterization of rock samples and mineralogical controls on leachates

By Jane M. Hammarstrom, Charles A. Cravotta III, Daniel Galeone, John J. Jackson, and Frank Dulong

Introduction

Rocks associated with coal beds typically include shale, sandstone, and (or) limestone. In addition to common rock-forming minerals, all of these rock types may contain sulfide and sulfate minerals, various carbonate minerals, and organic material. These different minerals have inherently different solubility characteristics, as well as different acid-generating or acid-neutralizing potentials. The abundance and composition of sulfur- and carbonate-bearing minerals are of particular interest in interpreting the leaching column data because (1) pyrite and carbonate minerals are the primary controls on the acid-base account of a sample, (2) these minerals incorporate trace metals that can be released during weathering, and (3) these minerals readily react during weathering due to mineral dissolution and oxidation of iron.

Rock samples were collected by the Pennsylvania Department of Environmental Protection (PaDEP) from five different sites to assess the draft standardized leaching column method (ADTI-WP2) for the prediction of weathering rates and water quality at coal mines. Samples were sent to USGS laboratories for mineralogical characterization and to ActLabs for chemical analysis. The samples represent a variety of rock types (shales, sandstones, and coal refuse) that are typical of coal overburden in the eastern United States. These particular samples were chosen for testing the weathering protocols because they represent a range of geochemical and lithologic characteristics, sulfur contents, and acid-base accounting characteristics (Hornberger et al., 2003). The rocks contain variable amounts of pyrite and carbonate minerals and vary in texture.

This chapter includes bulk rock chemical data and detailed mineralogical and textural data for unweathered starting materials used in the interlaboratory validation study, and for two samples used in the early phases of leaching column tests (Wadesville Sandstone, Leechburg Coal Refuse). We also characterize some of the post-weathering rock samples, report trace-element content in leachate, and discuss mineralogical controls on leachate quality based on data from one of the participating laboratories. Table 5.1 lists the samples described in this chapter, the sample numbers, and comments on the characteristics of each lithology. Sample locations are plotted in Figure 5.1. Chapters 2 and 3 describe the sample locations, sample preparation protocols, ABA characteristics, and rationale for selection of rock samples for testing. Microprobe data for pyrite and carbonate minerals are tabulated in Appendix 5.1. Leachate data, along with a series of graphs showing concentration and cumulative transport trends, for the laboratory data discussed in this chapter are included as Excel spreadsheets in Appendices 5.2 and 5.3. Leach column data for the interlaboratory study are evaluated and interpreted in Chapters 7 -11.

Table 5.1. Rock samples.

Sample	Lithology	Comment
HCS-IN	Houchin Creek Shale	• Low NP • High S • Produces alkaline mine discharge
LKFC-PA	Lower Kittanning Shale	• Low NP • Produces alkaline mine discharge
KBF-WV	Kanawha Black Flint Shale	• Low NP • Low S • Selenium problem area
BCS3-PA	Brush Creek Shale	• Moderate NP • Moderately high S • Produces alkaline mine discharge
MKSS	Middle Kittanning Sandstone	• Low NP • Low S • Low target analytes ("blank")
Wadesville #29	Wadesville Sandstone	• High NP • Low S • Produces alkaline mine drainage
LRBT#2	Leechburg Coal Refuse	• High S • High acidity end-member

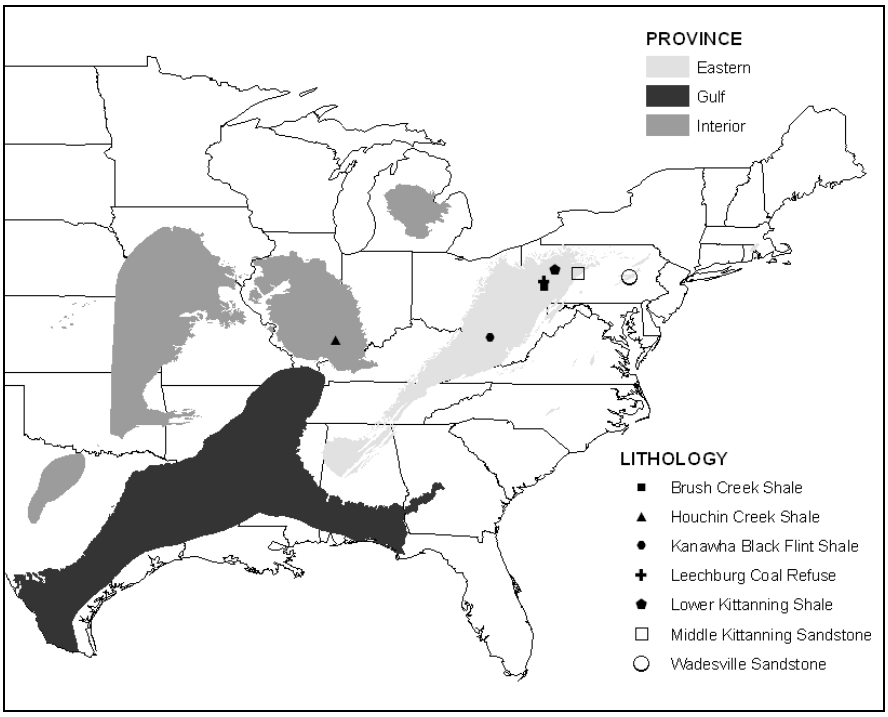

Figure 5.1 Sample location and major coal provinces of the eastern United States. .

Methods

Leach test starting materials were characterized by a number of methods, including whole-rock chemistry, optical microscopy, powder x-ray diffraction (XRD), scanning electron microscopy (SEM), and electron probe microanalysis (EPMA). Microscopy and XRD were used to identify the types of minerals present in each lithology and to estimate their relative abundances. Microbeam techniques (SEM and EPMA) were used to identify fine-grained minerals and determine mineral composition.

Splits of each rock sample were submitted to ActLabs for chemical analysis of major and trace elements using whole rock fusion ICP analysis (FUS-ICP), total digestion ICP analysis (TD-ICP), multi-element instrumental neutron activation analysis (MULTI-INAA), and high-temperature (>750 ^{o}C) loss-on-ignition (LOI). Mercury was determined by atomic absorption using a flow injection technique (FIMS); CO_2 was determined by coulometry (COUL). At the completion of the Phase 3 leaching column tests, one of the laboratories recovered the solid sample residue and supplied a split for testing. We sent a split of leach column residue (LCR) to ActLabs for carbon and sulfur analysis; another split was micronized for powder XRD for comparison with the mineralogy of the starting material. Leach column residues were analyzed for carbon and sulfur using automated analyzers (infrared detector). CO_2 was determined by treating a split with 25% HCl; graphitic carbon was determined by heating to 600 ^{o}C to drive off CO_2 and organic carbon. The difference between total carbon and the organic + CO_2 carbon fractions is reported as graphitic carbon. Details of analytical methods are available at the ActLabs website: http://www.actlabs.com/methods_usa.htm

Samples for mineralogical studies consisted of fresh splits (75 to 100 g) of the five particle size composites used for the phase 3 column experiments, plus unsized Wadesville sandstone and Leechburg Coal refuse (Table 5.1). The composites were split in the Reston laboratory by the cone and quarter method. Half of the sample was retained as an archive sample and half was split for XRD and other mineralogical studies (OMS split). The XRD split was subsampled, micronized in alcohol in a McCrone[1] mill equipped with agate grinding pellets to reduce average particle size to 1 to 5 micrometers, air dried, and analyzed as a powder XRD mount. Polished thin sections were prepared from rock chips (at least five 1-cm size chips per sample) selected from the OMS split.

Powder patterns were collected on a Scintag X1 automated diffractometer equipped with a Peltier detector using CuKa radiation. Patterns were interpreted with the aid of Scintag and MDI Applications JADE search/match software and compared with reference patterns in the Powder Diffraction File (ICDD, 2002). The relative amounts of different minerals were estimated by quantitative phase analysis using the Siroquant computer program (Taylor and Clapp, 1992). Siroquant utilizes the full XRD profile in a Rietveld refinement to estimate the weight percentages of different minerals in the mixture, based on a rigorous identification of minerals present prior to the refinement. Raudsepp and Pani (2003) summarized applications of Rietveld analysis for environmental studies of mine wastes. Small amounts (<5 weight percent) of a mineral are not always detectable by XRD. XRD cannot uniquely determine mineral composition; thus we report plagioclase, which may be calcic or sodic. Although we report both muscovite and phengite and illite micas, absolute concentrations of minerals are not reliable by

[1] Any use of trade, product, or firm names is for descriptive purposes only and does not imply endorsement by the U.S. Government.

these methods. The relative differences among mineral groups (micas, chlorite, quartz, carbonates, pyrite, and sulfates) are plotted because these are more reliable estimates of the mineralogical variation among the samples. Overlapping peaks of the many rock-forming minerals present in shales complicate mineral identification. Also, most rock-forming minerals form solid solutions so compositions may differ from the minerals in reference databases used to interpret XRD patterns. Uncertainties in XRD interpretation were resolved by optical and electron microscopy on thin sections, where possible.

Polished thin sections were prepared for each rock by mounting 6 to 12 fragments in colorless epoxy, affixing the cemented fragments to a glass slide, and grinding to a thickness of 30 micrometers. Polished sections were examined with a Nikon petrographic microscope equipped with both transmitted and reflected light. Sections were scanned and photographed to document grain size and texture and to provide reference maps for detailed microbeam analyses. Rock fragments in each polished section were assigned letter labels (A, B, C, etc.) for reference. Sections were coated with carbon and examined with a JEOL JSM-840 scanning electron microscope (SEM) equipped with a back-scattered electron (BSE) detector, a secondary electron (SE) detector, and a PGT x-ray energy-dispersive system (EDS). In BSE images, grayscale colors reflect average atomic number contrasts of minerals. Heavy minerals, such as pyrite or zircon, appear bright or white. Organic material appears black because it is mainly composed of the light element carbon. Other minerals appear in varying shades of gray. EDS spectra were collected to obtain qualitative analysis of mineral compositions to refine XRD identifications and choose appropriate starting minerals from the Siroquant mineral library for Rietveld refinement. The SEM typically was operated at an accelerating voltage of 15 kV and a specimen current of 1 to 2 nA. A JEOL electron microprobe (EMP) was used to analyze pyrite and carbonate minerals. For pyrites, the microprobe was operated at 20kV with a beam current of 30 nanoamps, using a focused beam and natural and synthetic sulfide minerals as standards. Long (60 second) count times were used to optimize detection limits for trace elements in pyrite (Se, Ni, As, Co, Mn, Cu, Zn, Cd). Detection limits for these elements are on the order of 100 parts per million (ppm). For carbonates, the microprobe was operated at 15kV with a beam current of 10 nanoamps, and a slightly defocused (5-micrometer) beam to minimize sample damage; natural and synthetic carbonate minerals were used as standards. The EPMA technique cannot determine carbon, water, or oxidation states of elements. Therefore, carbon dioxide contents for carbonate minerals are calculated based on stoichiometry.

Petrographic observations and SEM analyses showed that some samples contain organic matter. Non-crystalline (amorphous) materials are non-diffracting by powder x-ray analysis. We addressed the issue of non-diffracting material in two ways. We reran the XRD patterns after adding 15 weight percent corundum as an internal standard. This allowed us to use Siroquant to estimate the amount of non-diffracting material in each sample. The non-diffracting (amorphous) material includes organic material, poorly crystalline ferrihydrite or aluminum oxyhydroxide minerals, and any material rendered amorphous during sample preparation. We also subjected 1 gram powdered sample splits to a low-temperature ash (LTA) procedure to estimate the amount of non-mineral matter. The LTA analyses were done in USGS laboratories by radio-frequency plasma-ashing (Pontolillo and Stanton, 1994; Rao and Gluskoter, 1973; Mitchell and Gluskoter, 1976; Pearson and Kwong, 1979). XRD patterns for the LTA residues were analyzed using Siroquant to estimate mineral abundances for comparison with the pre-ash data.

The target analytes for the interlaboratory leach column tests were iron, manganese, aluminum, calcium, magnesium sodium, potassium, zinc, selenium, and sulfate (Chapter 8; Appendix 5.2). Leaching column effluent from the last two weeks of the 14-week weathering test at West Virginia University was submitted to ActLabs by Dr. Louis MacDonald for analysis of additional trace elements that might be released during weathering. The trace-element leachates were analyzed for 76 elements by ICP-MS, ICP-OES, and FIMS for mercury.

Results

Samples characterized in this study include four shales, two sandstones, and coal refuse (Table 5.1). The Wadesville Sandstone and Brush Creek Shale were used in phase 1 studies in 2002. The Brush Creek Shale and Leechburg Coal Refuse were used in phase 2 leaching column studies conducted in 2003 (Hornberger et al., 2004). The Brush Creek Shale and rocks from the Middle Kittanning Sandstone were used in phase 3 tests in 2006. The samples exhibit a wide range of geochemical characteristics in terms of percent total sulfur and neutralization potential, as described in previous publications (Hornberger et al, 2003, 2004; Hornberger and Brady, 1998, Brady et al, 1998). Acid-base accounting data are discussed in detail in Chapter 9.

Whole-rock chemistry

Geochemical data for the unweathered whole-rock samples are reported in Table 5.2, along with carbon and sulfur analyses obtained for weathered leach column residue from one laboratory. The chemistry of the leachate may not directly mimic the chemistry of the rocks because of differences in the solubilities and rates of reaction of various solid phases that contain the analytes. Variations in major rock constituents are illustrated in Figure 5.2*A*. The wide range in loss-on-ignition (<5 to 60 weight percent LOI) reflects the variable content of organic material and other volatiles. The Wadesville Sandstone contained significantly more calcium (11.23 weight percent CaO) and manganese than any of the other samples (Table 5.2). Total sulfur concentrations are negligible in the sandstones (<0.1 weight percent) and range from 0.2 to 4.3 weight percent in the shales. The coal refuse analyzed for this study contains over 5 weight percent sulfur (Table 5.2). Total sulfur does not correlate with total iron concentrations in the rocks. Sulfur concentrations overlap those reported in the separate ABA determinations (Chapter 9). The carbon dioxide (CO_2) content of the rocks indicates the carbonate mineral content. The shales contain 1 to 3 weight percent carbon dioxide; whereas, the Wadesville Sandstone contained 16.2 weight percent carbon dioxide. As discussed in more detail below, the Wadesville Sandstone had a substantially greater percentage of carbonate minerals than the other rocks. Concentrations of selected trace elements of potential environmental concern are plotted in Figure 5.2*B* on a log scale to facilitate comparison of samples. Relative to the other shales and sandstones, the Houchin Creek shale contains the highest concentrations of base metals (mostly zinc), arsenic, selenium, and mercury. The Leechburg coal refuse contains the highest concentration of mercury (952 parts per billion) detected in any of the samples.

Post-leaching carbon and sulfur data (Table 5.2) show that neither component was exhausted during the leaching study.

Table 5.2. Geochemical data for rock samples.
[Total iron reported as Fe_2O_3; n.d., not determined]

Lithology				Shale				Sandstone		Coal refuse
Sample				HCS-IN	LKFC-PA	KBF-WV	BCS3-PA	MKSS	Wadesville #29	LRBT #2
Element	Units	Detection Limit	Method							
				Major elements as oxides						
SiO_2	%	0.01	FUS-ICP	38.27	50.44	57.44	47.59	75.36	49.43	19.01
Al_2O_3	%	0.01	FUS-ICP	12.59	17.77	16.04	20.45	11.12	9.08	9.28
Fe_2O_3(T)	%	0.01	FUS-ICP	9.09	11.07	8.77	9.52	3.22	6.83	7.55
MnO	%	0.01	FUS-ICP	0.05	0.23	0.13	0.13	0.06	0.37	0.01
MgO	%	0.01	FUS-ICP	1.61	1.88	1.81	2.41	0.89	3.84	0.38
CaO	%	0.01	FUS-ICP	2.25	0.87	1.03	2.25	1.81	11.23	0.12
Na_2O	%	0.01	FUS-ICP	0.5	0.21	0.74	0.25	0.14	0.36	0.12
K_2O	%	0.01	FUS-ICP	2.75	3.68	3.44	3.51	2.4	1.5	1.04
TiO_2	%	0.005	FUS-ICP	0.574	0.861	0.884	0.848	0.653	0.526	0.498
P_2O_5	%	0.01	FUS-ICP	0.35	0.42	0.22	0.3	0.08	0.12	0.01
LOI	%	0.01	FUS-ICP	31.84	12.26	8.86	11.93	4.58	16.58	59.97
Total	%	0.01	FUS-ICP	99.89	99.69	99.37	99.19	100.3	99.86	98
				Trace elements						
Ag	ppm	0.5	INAA	1.2	< 0.5	< 0.5	< 0.5	< 0.5	< 0.5	< 0.5
As	ppm	2	INAA	48	22	8	30	4	4	56
Au	ppb	5	INAA	< 5	< 5	< 5	< 5	< 5	< 5	< 5
Ba	ppm	3	INAA	307	476	580	676	313	309	138
Be	ppm	1	FUS-ICP	4	4	3	4	2	2	2
Bi	ppm	2	TD-ICP	< 2	< 2	< 2	< 2	< 2	< 2	3
Br	ppm	1	INAA	< 1	< 1	< 1	< 1	< 1	< 1	6
Cd	ppm	0.5	TD-ICP	20	< 0.5	< 0.5	< 0.5	< 0.5	< 0.5	< 0.5
Ce	ppm	3	INAA	59	103	90	93	57	61	51
Co	ppm	1	INAA	19	24	16	23	11	15	5
Cr	ppm	1	INAA	179	88	77	101	87	45	51
Cs	ppm	0.5	INAA	6.6	6.6	4.6	8.2	1.9	1.1	4.3
Cu	ppm	1	TD-ICP	117	32	27	77	12	15	28
Eu	ppm	0.1	INAA	1.3	2.1	1.8	1.5	1.1	1	0.7
Hf	ppm	0.5	INAA	2.1	4.8	5.9	2.9	4.4	4.4	2.3
Hg	ppm	1	INAA	< 1	< 1	< 1	< 1	< 1	< 1	1
Hg	ppb	5	FIMS	227	63	11	65	11	< 5	952
Ir	ppb	5	INAA	< 5	< 5	< 5	< 5	< 5	< 5	< 5
La	ppm	0.2	INAA	35.4	53.2	52.6	52.7	31.7	35	25.5
Lu	ppm	0.05	INAA	0.36	0.63	0.6	0.53	0.36	0.34	0.3
Mo	ppm	5	INAA	165	< 5	< 5	< 5	< 5	< 5	< 5
Nd	ppm	5	INAA	26	38	43	40	24	28	18
Ni	ppm	1	TD-ICP	235	64	38	83	23	18	22
Pb	ppm	5	TD-ICP	27	24	22	46	20	15	22
Rb	ppm	20	INAA	80	100	110	120	70	70	50
Sb	ppm	0.2	INAA	13.2	0.9	0.5	0.9	0.4	< 0.2	0.8
Sc	ppm	0.1	INAA	11.9	18.5	15.1	19.4	8.8	9.3	9.9
Se	ppm	3	INAA	81	< 3	< 3	< 3	< 3	< 3	13
Sm	ppm	0.1	INAA	6	10.4	9.2	8.4	5.2	6.1	4
Sr	ppm	2	FUS-ICP	118	108	122	163	66	113	112
Ta	ppm	1	INAA	< 1	< 1	< 1	1	< 1	< 1	< 1
Tb	ppm	0.5	INAA	< 0.5	< 0.5	1.1	0.9	< 0.5	< 0.5	< 0.5

Table 5.2.—Continued.

Lithology				Shale				Sandstone		Coal refuse
Sample				HCS-IN	LKFC-PA	KBF-WV	BCS3-PA	MKSS	Wadesville #29	LRBT #2
Th	ppm	0.5	INAA	5.7	8.8	8.9	9.7	5.3	4.6	5.4
U	ppm	0.5	INAA	37.7	3.5	3	4.3	1.7	1.3	2.2
V	ppm	5	FUS-ICP	695	157	114	218	66	64	64
W	ppm	3	INAA	< 3	< 3	< 3	< 3	< 3	< 3	< 3
Y	ppm	1	FUS-ICP	31	43	39	33	21	25	14
Yb	ppm	0.1	INAA	2.3	3.8	4.1	3.3	2.3	2.7	1.8
Zn	ppm	1	TD-ICP	456	151	126	171	86	50	33
Zr	ppm	2	FUS-ICP	92	182	248	132	199	183	67
CO_2	%	0.01	COUL	1.06	3.13	1.94	2.03	1.93	16.2	1.06
S	%	0.001	TD-ICP	4.33	0.815	0.207	0.538	0.089	0.017	5.54
Carbon and sulfur analyses on leach column residues										
C_{Total}	%	0.01	IR	18.1	2.53	1.07	1.69	0.79	n.d.	n.d.
$C_{Graphite}$	%	0.05	IR	4.32	0.47	0.19	0.43	< 0.05	n.d.	n.d.
$C_{Organic}$	%	0.05	IR	13.7	1.15	0.52	0.65	0.06	n.d.	n.d.
CO_2	%	0.01	COUL	0.41	3.34	1.3	2.24	2.52	n.d.	n.d.
S	%	0.01	IR	4.88	0.98	0.19	0.55	0.09	n.d.	n.d.
SO_4	%	0.1	IR	1.4	0.4	0.5	1	0.2	n.d.	n.d.

Rock Descriptions: Textures and Mineralogy

Mineralogical data are discussed by rock type. Mineralogy and rock textures for each lithology are illustrated by a series of photomicrographs and SEM images of polished thin sections. Shales and sandstones incorporate a variety of minerals, including different varieties of mineral groups (clays, feldspars). Ankerite, for example, is an iron-bearing variety of dolomite. The term ankerite is used for dolomite-group minerals that have $Fe^{2+}/(Mg+Fe^{2+}) \geq 0.2$. Table 5.3 lists nominal minerals compositions; however, many common rock-forming minerals such as feldspars and micas have variable compositions because they form solid solutions. Also, individual crystals of a single mineral may be compositionally zoned.

Pyrite occurs mainly as framboids in the samples. The term framboid (from the French "framboise") refers to the raspberry-like texture of the pyrite. Framboids are spherical structures made up of equant microcrystals of pyrite.

Estimated mineral abundances for the raw leach column starting material as determined by Siroquant are summarized in Table 5.4, along with data for samples after the low-temperature ash (LTA), leach column residues, estimated amorphous content and measured % LTA. Some trace minerals identified by SEM were not identified by XRD because of their low modal abundance. Estimates of low concentrations (<5 weight percent) of minerals by XRD are not very reliable; errors on individual minerals are on the order of $\pm$ 1 weight percent.

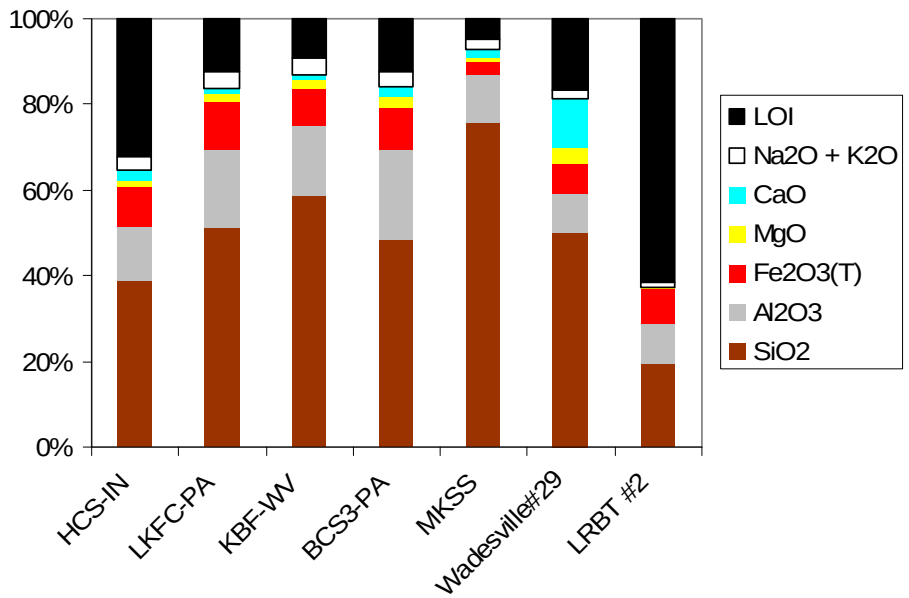

Figure 5.2*A*. Bar chart showing relative proportions of major elements as oxides and loss on ignition (LOI) based on whole-rock geochemical data for unweathered rocks (Table 5.2). Fe_2O_3(T) represents total iron reported as ferric iron.

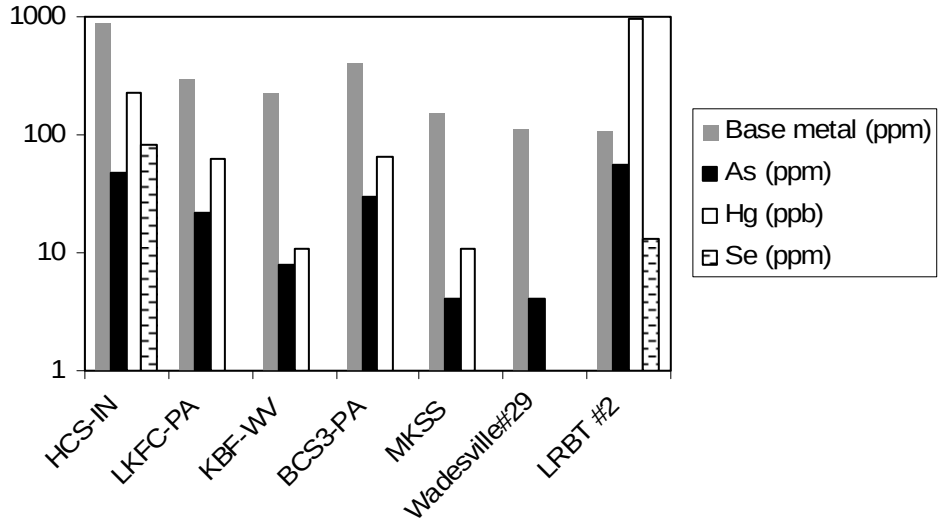

Figure 5.2*B*. Bar chart showing concentrations of selected trace-elements based on whole-rock geochemical data for unweathered rocks (Table 5.2). Base metals = Copper + lead + zinc+ cobalt + cadmium + nickel. Note that the data are plotted on a logarithmic scale. Selenium is below detection limits for all samples except HCS-IN and LRBT#2. Mercury is below detection limits for Wadesville #29.

Table 5.3. Minerals.
[Weathering behavior comments based on Goldrich's (1938) mineral-stability series in weathering and Sverdrup's (1990) relative reactivity of monomineralic samples; NP classes based on Jambor et al. (2002)]

Mineral	Ideal formula	Weathering behavior	NP<0	Inert	NP>0
Quartz	SiO_2	Inert		X	
Chlorite	$(Mg,Fe)_5Al(Si_3Al)O_{10}(OH)_8$	Intermediate weathering			X
Micas and clays					
Muscovite	$KAl_2(AlSi_3O_{10})(OH)_2$	Very slow weathering		X	
Phengite	Series between muscovite and $K(Mg,Fe^{2+})(Al,Fe^{3+})Si_4O_{10}(OH)_2$			X	
Biotite	$K(Mg,Fe)_3(AlSi_3O_{10})(OH)_2$	Intermediate weathering			X
Illite	$K_{0.65}Al_2(Al_{0.65}Si_{3.35}O_{10})(OH)_2$	Very slow weathering			
Kaolinite	$Al_2Si_2O_5(OH)_4$	Slow weathering		X	
Feldspars					
Albite	$NaAlSi_3O_8$	Slow weathering		X	
Anorthite	$CaAl_2Si_2O_8$	Fast weathering		X	X
Potassium feldspar	$KAl_2(AlSi_3O_{10})(OH)_2$	Very slow weathering		X	
Accessory minerals					
Apatite	$Ca_5(PO_4)_3(OH,F,Cl)$	Fast weathering			X
Zircon	$ZrSiO_4$	Inert		X	
Rutile	TiO_2	Inert		X	
Sulfate minerals					
Gypsum	$CaSO_4 \bullet 2H_2O$			X	
Barite	$BaSO_4$	Insoluble		X	
Sulfide minerals					
Pyrite	FeS_2		X		
Carbonate minerals					
Calcite	$CaCO_3$	Dissolving			X
Siderite	$FeCO_3$	Dissolving	X		X
Ankerite	$Ca\ (Fe,Mg,Mn)(CO_3)_2$	Dissolving	X		X

Houchin Creek Shale (Sample HCS-IN). The Houchin Creek Shale was selected for weathering experiments because of its high total sulfur content and low NP values (Table 5.1). In thin section, the shale is a black, very fine-grained homogeneous rock; one of the eight fragments contained clots and veinlets of coarse-grained calcite (Figure 5.3). The shale contains significant amounts of organic material, as indicated by thin section and SEM observations (Figure 5.4) and the low-temperature ash measurement of 79 weight percent. Sample HCS-IN also had the highest LOI of all the shales. The post-leach residue contained 18.1% total carbon, most of which is organic (Table 5.2). The crystalline part of the shale was composed of ~32% quartz, 26% micas and clay minerals, 5% chlorite, 17% pyrite, 6% feldspar, ~ 3% carbonate minerals, gypsum, and accessory minerals (Table 5.4). The XRD-based estimate of amorphous content of the shale was 67 weight percent (Table 5.4). Pyrite is scattered throughout the shale as single grains or as clusters of framboids (Figure 5.3*D*). Most of the minerals were so fine-grained that they cannot be readily identified by optical microscopy. SEM images showed that the quartz was present as rounded grains on the order of 5 to 10 micrometers in diameter in a matrix of micas, clays, and other minerals (Figure 5.4).

Table 5.4. Mineralogy determined by XRD.

[Raw, raw sample of leach column starting material; LTA, sample after low-temperature ash to remove organic material; LCR, leach column residue after 16 weeks leaching. Data reported as weight percent of crystalline part of the rock. For each mineral, the error of the fit is on the order of ± 1 weight percent or less. Amorphous content estimated by Rietveld refinement on corundum-spiked samples. '-', not included in refinement

	HCS-IN			LKFC-PA			KBF-WV			BCS3-PA		
	Raw	LTA	LCR	Raw	LTA	LCR	Raw	LTA	LCR	Raw	LTA	LCR
Chi^{2*}	3.68	3.13	3.3	3.53	3.29	3.47	4.03	3.34	2.9	3.79	3.6	3.49
Mineral												
Quartz	32.4	30.7	34.3	37.1	36.8	40.0	42.0	42.2	39.7	34.4	32.2	33.7
Chlorite	5.0	4.2	4.6	9.9	9.0	8.9	6.2	8.9	6.3	10.9	11.4	7.2
Muscovite	7.8	14.2	8.4	16.4	17.1	12.0	15.7	15.3	15.2	16.8	19.8	18.0
Phengite	4.6	4.4	5.7	3.7	11.3	11.5	10.3	12.9	16.0	6.8	10.5	20.1
Biotite	-	-	-	-	-	-	0.1	0.8	1.7	-	-	-
Illite	11.6	7.7	12.9	9.5	4.6	8.4	2.3	1.6	2.7	8.6	8.4	6.5
Kaolinite	2.4	3.2	3.4	4.6	3.7	5.9	5.4	3.5	4.3	5.2	5.6	3.8
Micas & clay	26.4	29.5	30.4	34.2	36.7	37.8	33.8	34.1	39.9	37.4	44.3	48.4
Albite	4.5	4.3	4.4	0.0	0.0	0.0	9.3	6.2	3.5	0.0	0.0	0.0
Anorthite	0.9	2.5	0.6	1.6	0.1	0.1	0.8	0.1	0.1	0.2	0.1	0.1
Potassium feldspar	0.3	0.8	0.0	1.4	0.0	0.0	1.2	0.0	1.4	1.6	0.8	0.0
Feldspars	5.7	7.6	5	3	0.1	0.1	11.3	6.3	5	1.8	0.9	0.1
Apatite	3.3	6.4	3.5	1.5	2.4	0.1	0.4	1.5	0.9	0.0	0.2	2.2
Zircon	0.6	0.5	0.5	0.5	0.1	0.6	0.0	0.2	0.4	0.9	0.4	0.5
Rutile	0.0	0.5	0.3	0.7	0.4	0.6	0.8	1.1	0.4	0.7	0.9	1.3
Accessory minerals	3.9	7.4	4.3	2.7	2.9	1.3	1.2	2.8	1.7	1.6	1.5	4
Gypsum	6.4	0.0	9.1	0.0	0.0	0.6	0.0	0.0	0.4	0.0	0.0	0.0
Barite	0.0	0.0	0.1	0.2	0.0	0.1	0.7	0.2	0.0	0.9	0.3	0.0
Pyrite	17.5	17.3	11.2	7.5	7.9	2.4	0.8	1.3	0.9	3.0	3.4	3.0
Calcite	0.6	0.6	0.1	0.0	0.7	0.0	0.4	0.9	0.7	2.9	2.0	1.7
Siderite	0.0	0.3	0.0	5.0	4.8	8.4	3.1	1.8	5.2	4.7	3.9	1.5
Ankerite	2.1	2.7	0.9	0.3	1.1	0.2	0.7	1.6	0.3	2.4	0.0	0.4
Carbonate minerals	2.7	3.5	1	5.3	6.6	8.6	4.2	4.3	6.2	10.0	5.9	3.6
Amorphous content	69%			53%			51%			57%		
Low temperature ash (LTA)		79%			99%			99%			100%	
% Mass lost by LTA		21%			1%			1%			0%	
%LOI (chemistry)	32%			12%			9%			12%		

* Chi^2 is a computed statistical residual, which is used as a measure of the fit of the refinement of the XRD pattern. Chi^2=1 for a perfect correspondence between the least-squares model and the observed data. In complex rocks, ideal values are almost never observed due to systematic errors and imperfect physical corrections. Values less than 5 are considered reasonable fits for these rocks.

Table 5.4—Continued.

	MKSS			Wadesville #29		LRBT	
	Raw	LTA	LCR	Raw	LTA	Raw	LTA
Chi^{2*}	3.7	3.97	3.03	3.51	3.5	4.2	3.68
Quartz	64.5	58.9	61.7	41.62	41.7	22.98	23.16
Chlorite	4.3	6.0	5.4	3.73	3.24	2.13	1.77
Muscovite	13.8	8.3	13.6	2.54	6.79	7.27	8.3
Phengite	2.2	4.6	3.3	2.65	2.46	0.55	0.55
Biotite	-	-	-	-	-	-	-
Illite	0.5	3.6	3.7	1.7	1.4	14.91	13.68
Kaolinite	1.8	2.3	3.2	1.87	0.28	10.41	13.02
Micas & clay	18.3	18.8	23.8	8.76	10.93	33.14	35.55
Albite	0.3	1.4	0.5	2.6	0.87	0.01	0.02
Anorthite	1.5	2.0	0.0	0.5	1.11	4.35	3.01
Potassium feldspar	0.4	1.0	0.5	0.78	0.94	0.02	0.02
Feldspars	2.2	4.4	1	3.88	2.92	4.38	3.05
Apatite	0.6	1.2	0.9	1.89	0.7	3.89	2.9
Zircon	0.5	0.9	0.2	0.3	0.13	0.65	1.28
Rutile	1.0	1.2	0.9	1.04	0.52	0.63	1.23
Accessory minerals	2.1	3.3	2	3.23	1.35	5.17	5.41
Gypsum	0.0	0.0	0.0	0	0	0.5	0.88
Barite	0.4	0.5	0.5	0.01	0.11	0.62	0.02
Pyrite	0.4	0.7	0.5	0.91	0.53	29.08	29.02
Calcite	3.8	3.1	3.8	1.39	1.02	0.76	0.03
Siderite	2.5	2.9	1.2	0.3	0.06	0.02	0.2
Ankerite	1.6	1.5	0.2	36.1	38.1	1.21	0.88
Carbonate minerals	7.9	7.5	5.2	38	39	2.0	1.1
Amorphous content	37%			15%		77%	
Low temperature ash (LTA)		91%		100%		45%	
% Mass lost by LTA		9%		0%		55%	
%LOI (chemistry)	5%			17%		60%	

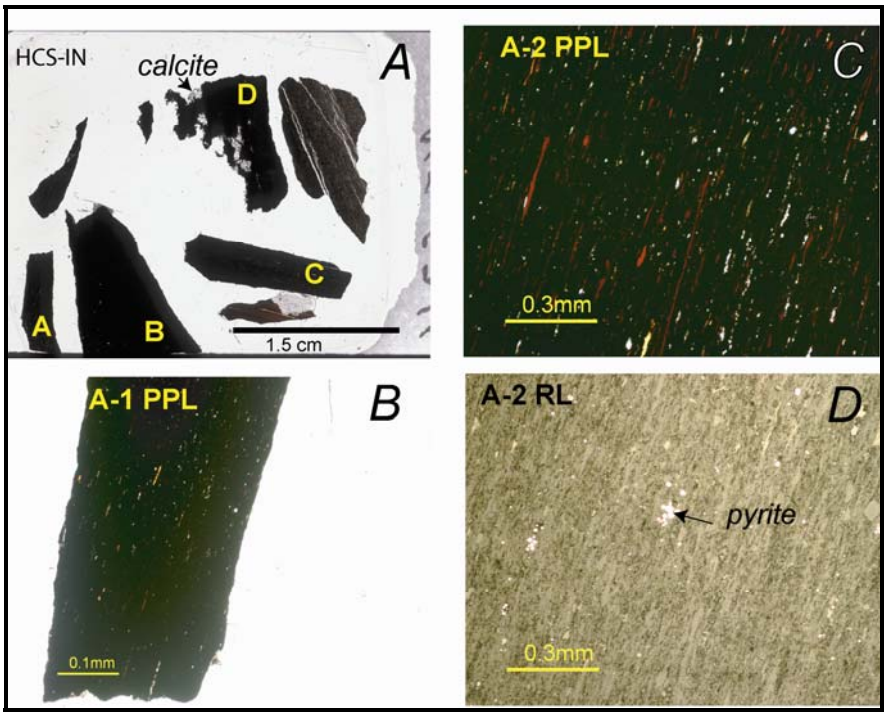

Figure 5.3. Houchin Creek Shale (Sample HCS-IN). *A*, Scanned image of polished thin section. Colorless patches on the edges of rock chip D are inclusions of calcite. ***B,*** Photomicrograph of rock chip A in plane-polarized light (PPL) showing the very fine-grained texture of the shale. *C*, Rock chip A at higher magnification. *D*, Same view of rock chip A as shown in *C* in reflected light (RL) shows clusters of pyrite framboids.

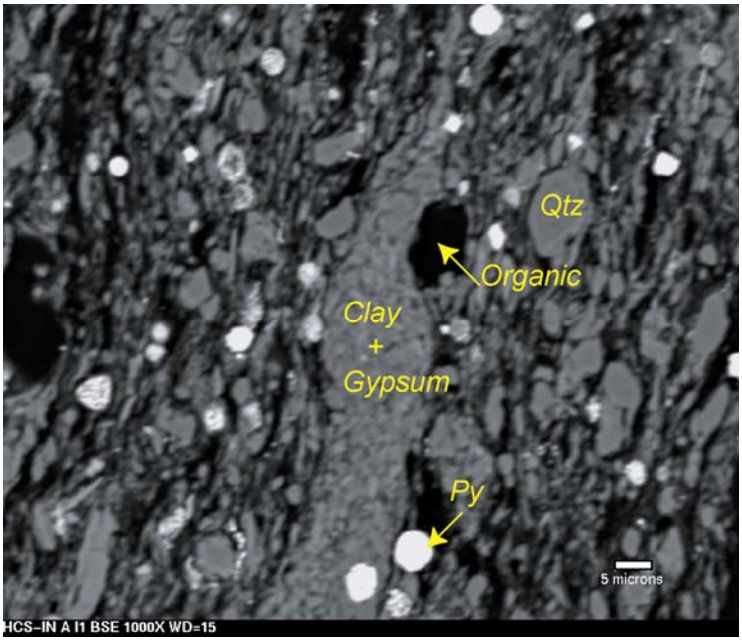

Figure 5.4. Houchin Creek Shale (Sample HCS-IN). SEM image of rock chip A in Figure 5.3 at 1,000X showing pyrite (Py, white) and organic material (black) scattered throughout the shale. BSE (backscatter mode) shows the atomic number contrast of different minerals. Quartz (qtz) appears gray.

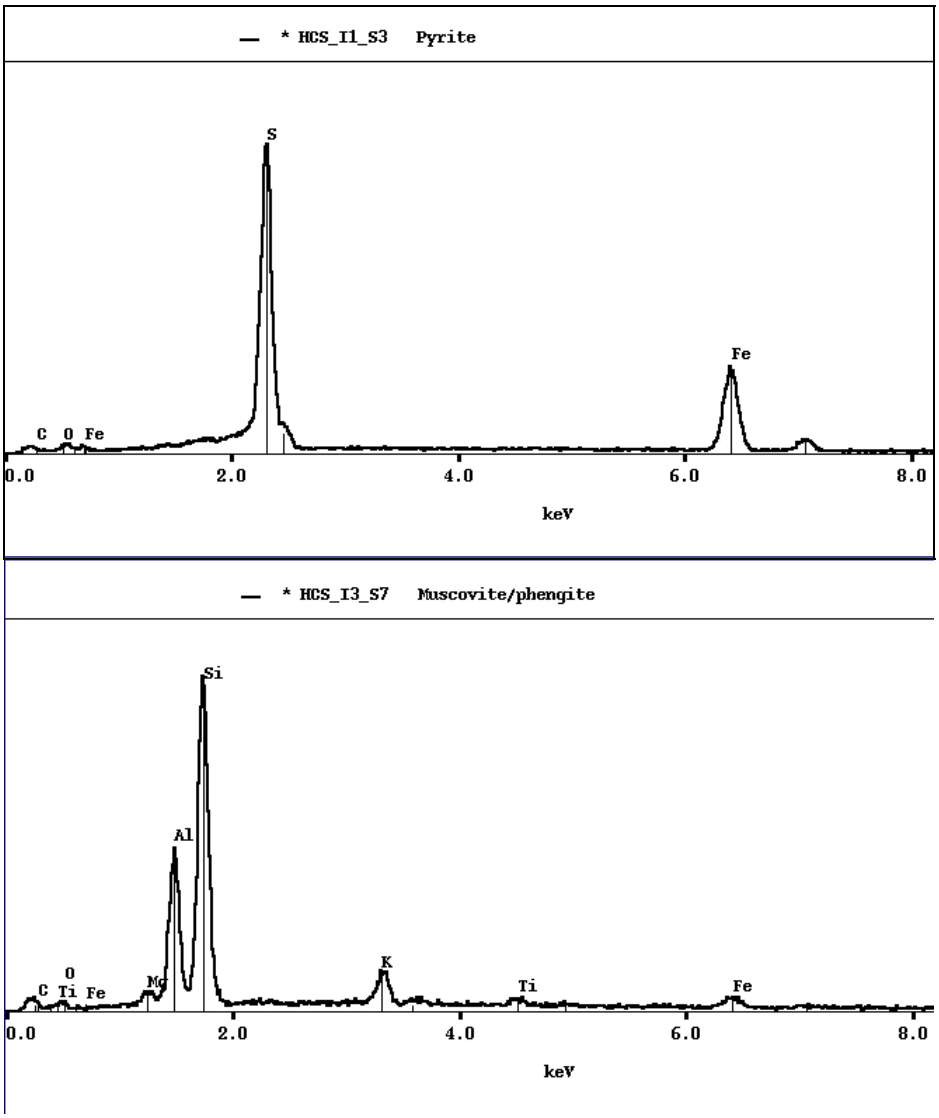

Figure 5.5. Houchin Creek Shale (Sample HCS-IN). EDS spectra for pyrite and muscovite (phengite). The EDS spectra show the elemental compositions at discrete spots in polished thin sections. The vertical bars are the reference positions for characteristic x-ray lines in electronvolts (keV). Pyrite is indicated by iron (Fe) peaks between 6 and 8 keV and sulfur (S) peaks just above 2keV. Muscovite is indicated by peaks for silicon (Si), aluminum (Al), potassium (K) with minor peaks for magnesium (Mg), iron (Fe) and titanium (Ti). Carbon (C) is detected because the samples are carbon-coated for analysis; traces of oxygen (O) are always present.

SEM spectra confirm identification of pyrite and show that some of the muscovite in HCS-IN contains minor amounts of iron and titanium, which agrees with the XRD identification of phengite (Figure 5.5). Carbon-rich organic material contains sulfur. The sulfur may be present as finely disseminated pyrite too small to be resolved by SEM. The SEM study confirmed the presence of gypsum and apatite, and also identified trace amounts of chalcopyrite.

Lower Kittanning Shale (Sample LKFC-PA). The Lower Kittanning Shale sample was collected from the Redbank Creek watershed in Pennsylvania, where overburden produces alkaline drainage although the NP is not very high. Sample LKFC contains about 1 weight percent sulfur and low NP. The Lower Kittanning Shale is coarser grained than the Houchin Creek Shale. Rock chips exhibit a range of textures in thin section. Some rock chips contain quartz grains up to 0.1 millimeters in diameter (Figure 5.6, chips A,B,C,F), some have more uniform, finer-grained , textures, and one chip (G) contained fossils. LKFC has low whole-rock loss-on-ignition and a low-temperature ash concentration of 99 weight percent indicating low total organic content. The XRD-based estimate of amorphous content of the shale is 67 weight percent (Table 5.2). The crystalline part of the shale is composed of the following (in weight percent): ~37 % quartz, 34 % micas and clay minerals, 10% chlorite, 8% pyrite, 3% feldspar, and 5% carbonate minerals (Table 5.4). Pyrite occurs as isolated cubes and as framboids scattered throughout all of the rock chips (Figure 5.7). Accessory minerals include apatite, which accounts for much of the phosphorous and some of the calcium in the rock. Although apatite is an accessory mineral present in low concentrations, apatite has NP>0 and can provide acid neutralization, especially where it is in close proximity to reacting pyrite (Figure 5.8). Framboids occur as rounded clusters of hundreds of discrete grains and as strings of crystals arranged like peas in a pod within organic material (Figure 5.9). These textures indicate an abundance of pyrite surfaces available for oxidation. Siderite is the dominant carbonate mineral identified by XRD. The siderite is not readily identified by optical microscopy because it is so fine-grained. Of the 18 rock chips examined, only chip G contained calcite, which is present as fossil material (Figure 5.10).

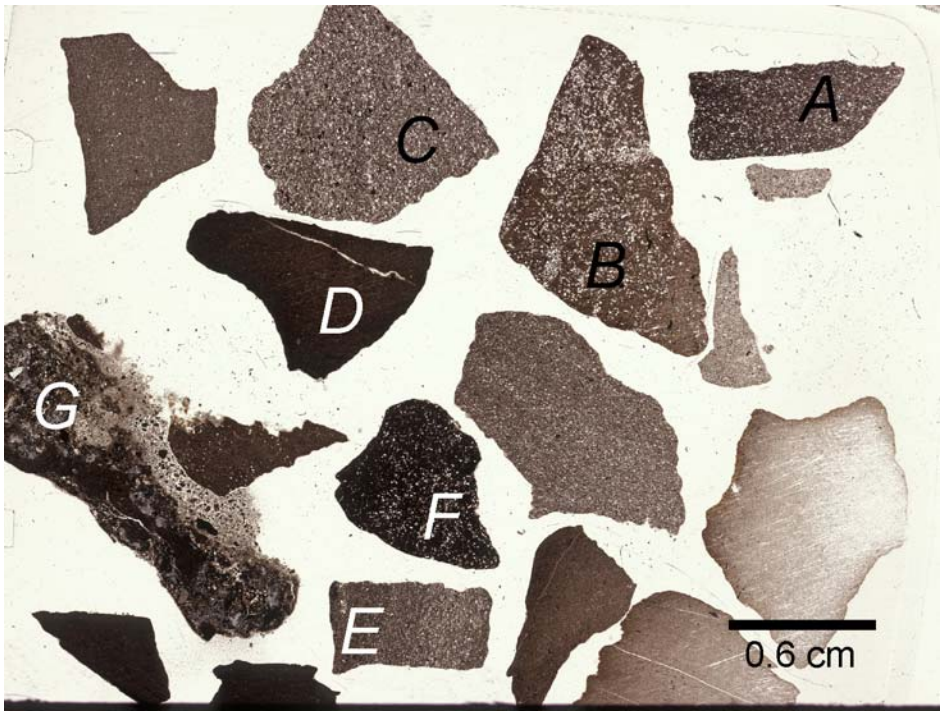

Figure 5.6. Lower Kittanning Shale (Sample LKFC-PA). Scanned image of polished thin section. Note the heterogeneous texture the different chips.

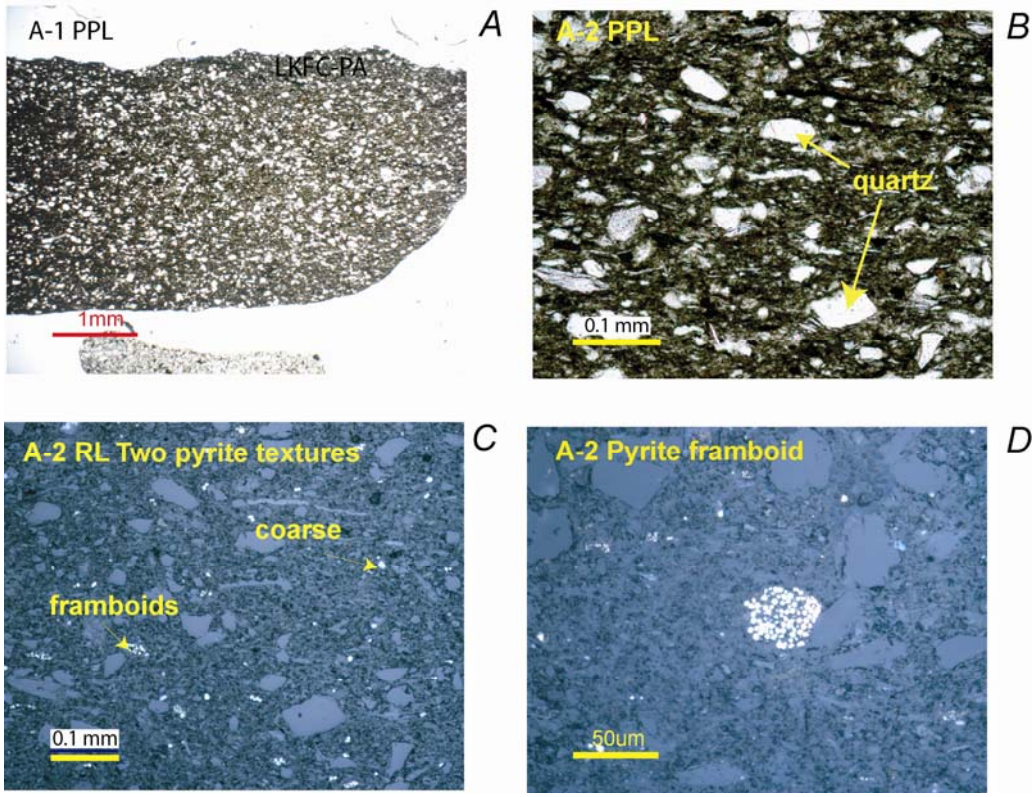

Figure 5.7. Lower Kittanning Shale (Sample LKFC-PA). Photomicrographs. A, Rock chip in plane-polarized light (PPL) at 2.5X. *B,* Subrounded quartz grains (0.1 millimeters across) in a fine-grained matrix mostly composed of mica, chlorite, and clay (20 X, PPL). *C*, Same view as *B*, in reflected light, shows scattered cubes of pyrite as well as framboids. *D,* High-magnification (50X) shows framboid texture, reflected light.

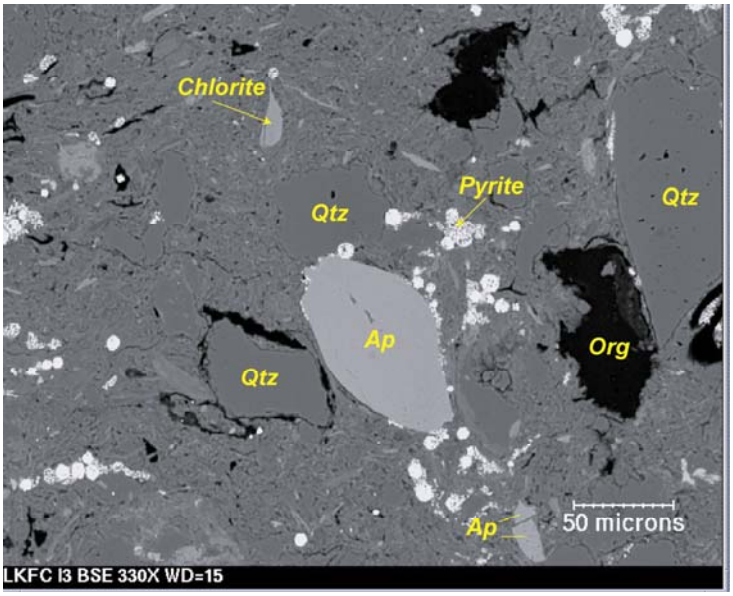

Figure 5.8. Lower Kittanning Shale (Sample LKFC-PA). SEM image showing coarse apatite rimmed by pyrite.

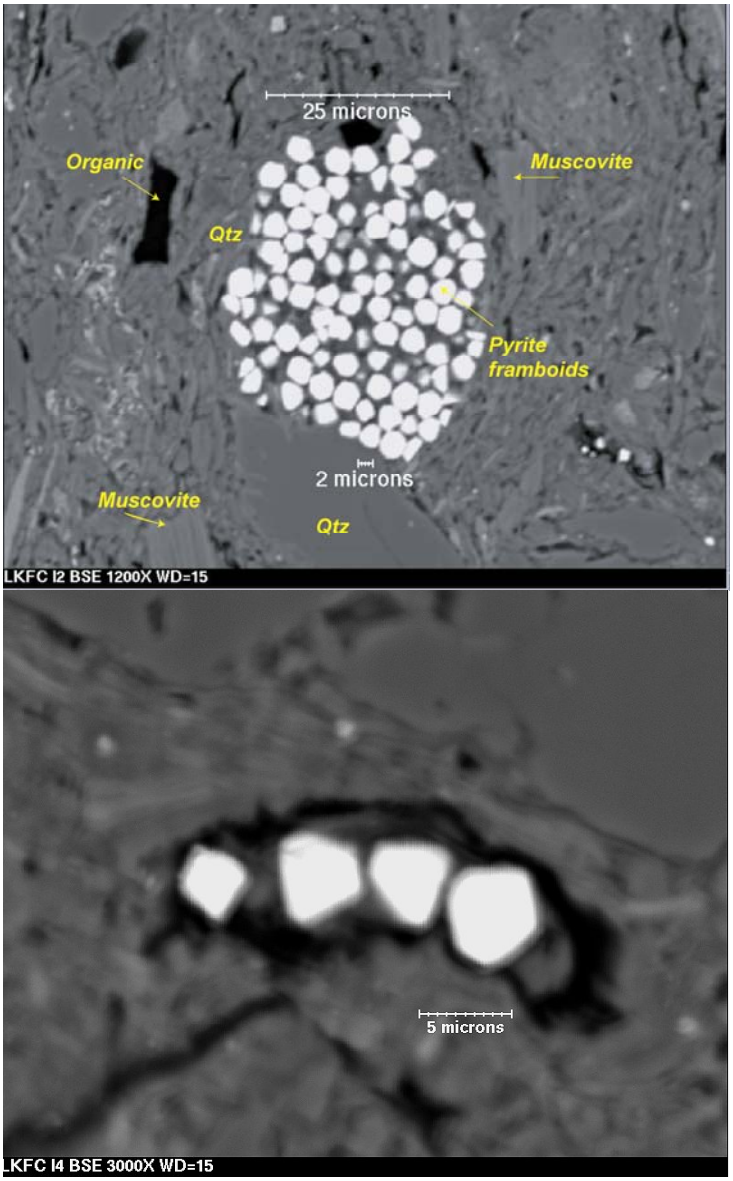

Figure 5.9. Lower Kittanning Shale (Sample LKFC-PA). SEM images of pyrite framboids. Note the large surface area. Rounded clusters on the order of 25 micrometers in diameter may consist of tens to hundreds of individual grains.

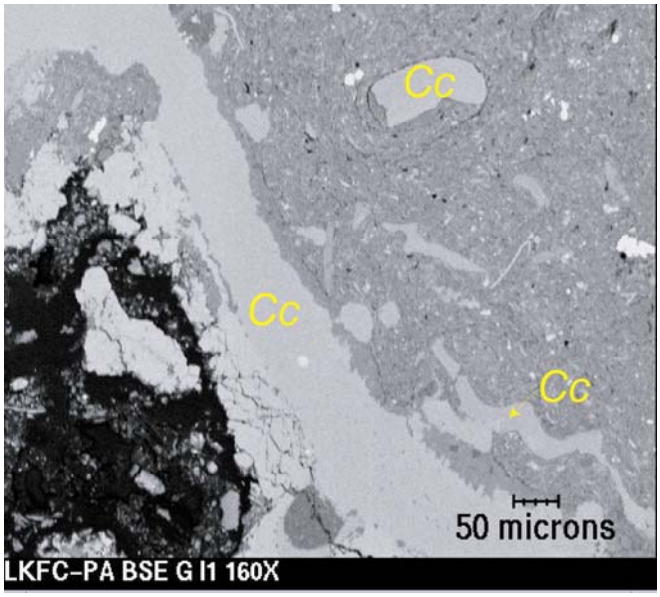

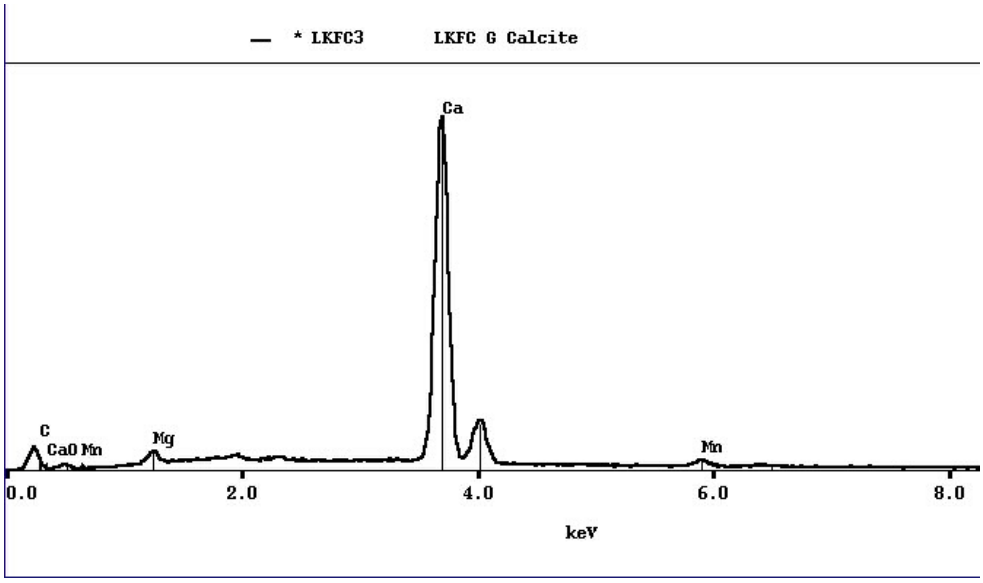

Figure 5.10. Lower Kittanning Shale (Sample LKFC-PA). SEM data showing BSE image of coarse calcite(Cc) in rock chip G. Note that the calcite contains minor amounts of Mg and Mn.

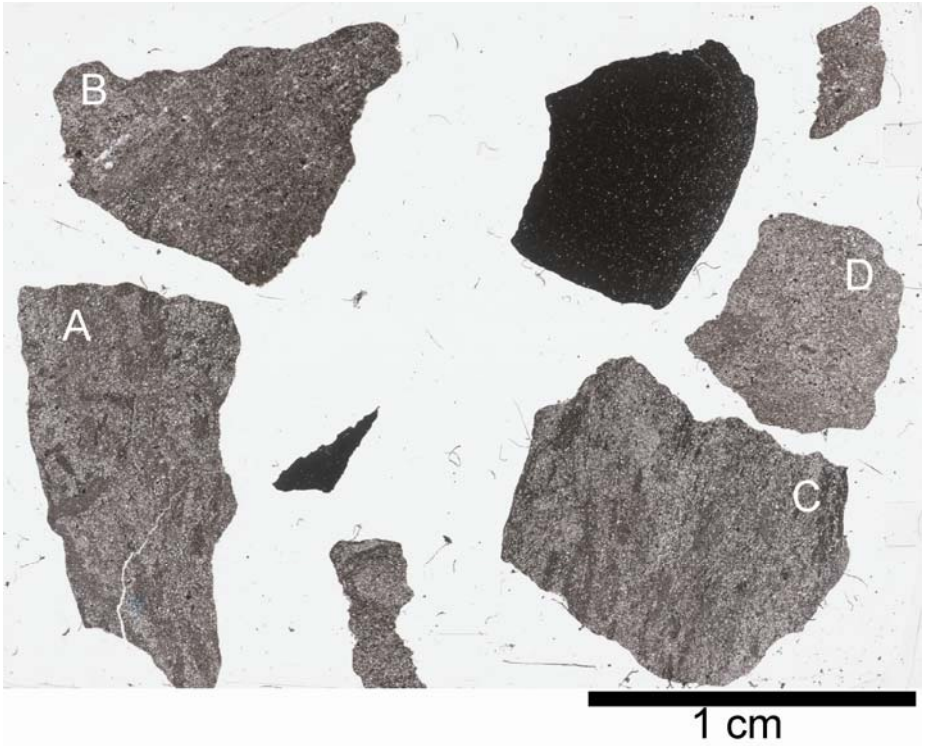

Figure 5.11. Kanawha Black Flint Shale (Sample KBF-WV). Scanned image of polished thin section.

Kanawha Black Flint Shale (Sample KBF-WV). The Kanawha Black Flint Shale was included in the phase 3 tests as a "gray-zone" sample from an area in West Virginia that might contain elevated selenium (Table 5.1). Gray zone samples are those samples for which alkalinity or acidity production is difficult to predict because of moderate amounts of neutralization potential and sulfur. The shale had low NP and contained about 0.2 weight percent sulfur. The selenium content of composite sample analyzed for this studied was below the detection limit (<3 parts per million selenium).

The shale is a patchwork of dark-colored clay-rich areas and coarser-grained quartz-rich areas (Figure 5.11). Low temperature ash (99 weight percent) and a relatively low loss-on-ignition (9 weight percent) indicate a relatively low organic content. XRD analysis estimated the mineralogical composition (in weight percent) as: 42 % quartz, 34% micas and clay minerals, 6% chlorite, <1% pyrite, 11% feldspar, and 4% carbonate minerals (Table 5.4). Laths of colorless muscovite, brown biotite, green chlorite and clots of brownish clay in a carbonate matrix were readily identifiable by optical microscopy (Figure 5.12). Despite the low estimates of organic material and pyrite for the bulk rock, both were present in many of the rock chips. The shale was more sodic (0.74 weight percent Na_2O) than the other samples (Table 5.2). It was also the most feldspathic (Table 5.4). Microprobe analysis confirmed the XRD identification of albite as the major feldspar present. Both Fe-rich carbonate and calcite were identified by SEM (Figure 5.13). Matrix carbonate grains (on the order of 5 micrometers or smaller) were slightly zoned, with iron increasing towards the rim of the grain. Zoned carbonate rimming a sphalerite grain explained the zinc detected in the whole-rock chemistry. Nearly pure calcite fragments (20 micrometers long) are rimed by pyrite (Figure 5-13).

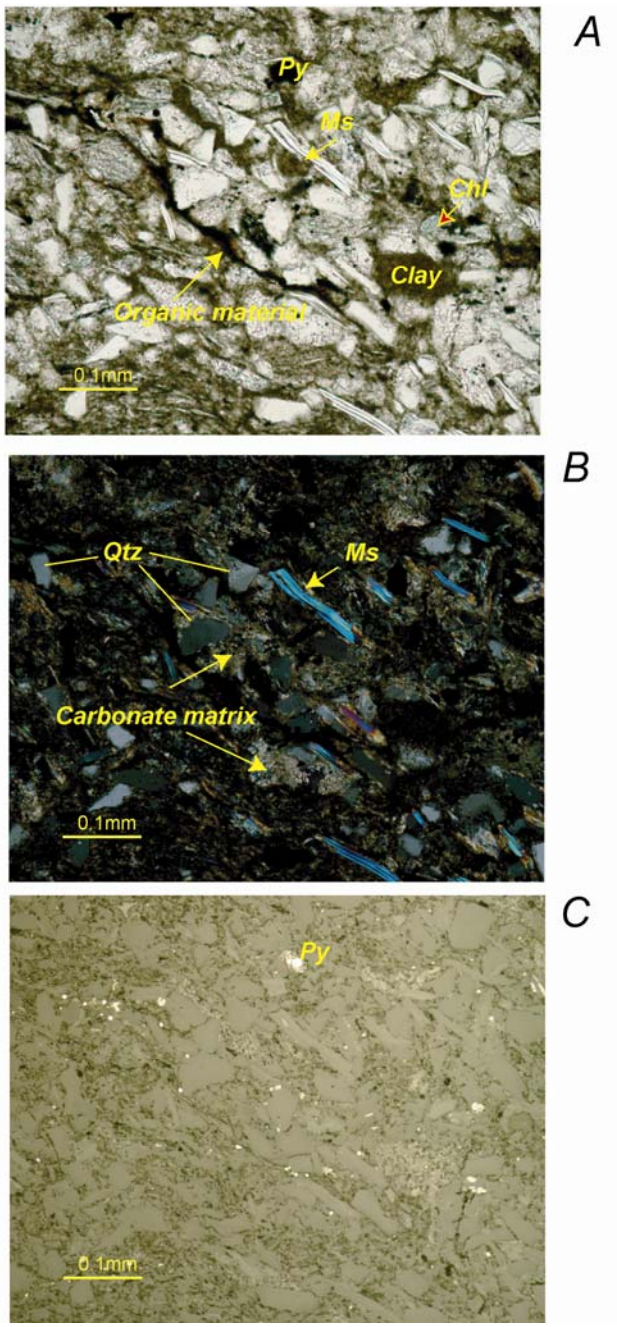

Figure 5.12. Kanawha Black Flint Shale (Sample KBF-WV). Photomicrographs of rock fragment C (Fig. 4). *A*, Quartz grains (Qtz), muscovite laths (Ms), green chlorite (Chl), clots of brown clay, pyrite (Py), and organic material; plane-polarized light. *B*, Same view in crossed nicols shows birefringence of carbonate-rich rock matrix. *C*, Same view in reflected light. All of the white grains are pyrite (Py). Note that both pyrite and organic material appear opaque (black) in transmitted light and some pyrite is enclosed in organic material.

A

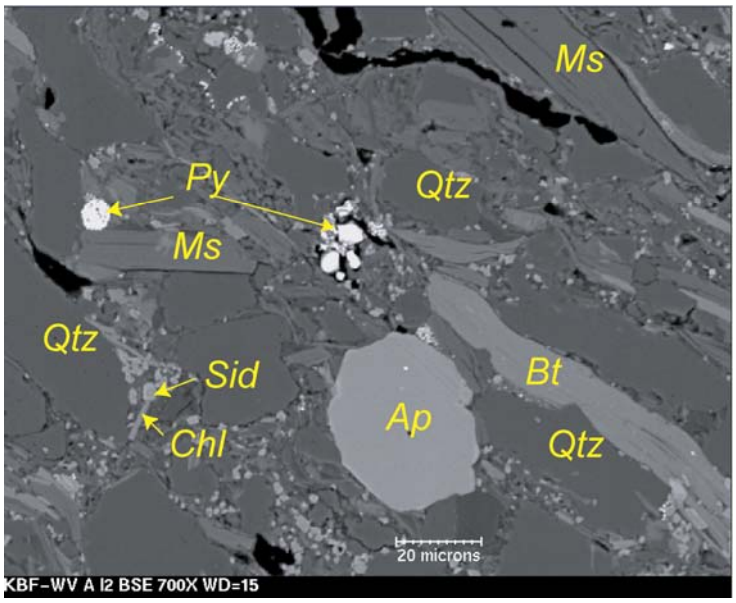

B

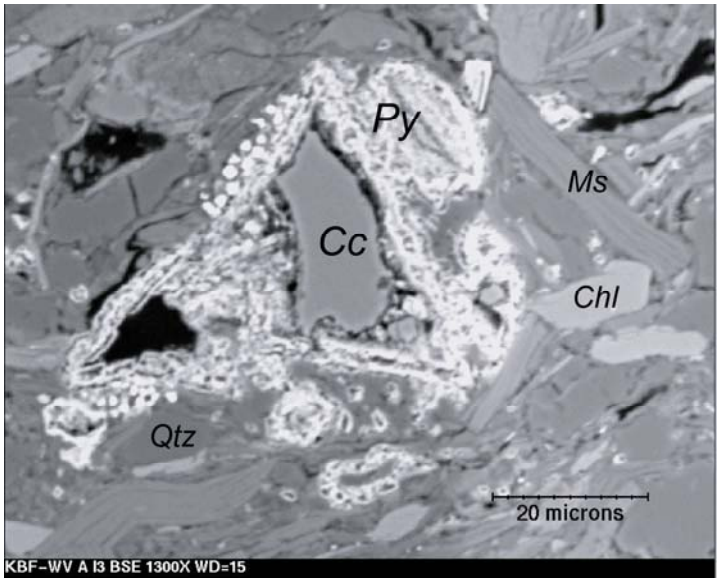

Figure 5.13. Kanawha Black Flint Shale (Sample KBF-WV). Backscattered-electron SEM images showing pyrite textures. *A*, Round pyrite framboid (6 micrometers in diameter) and clot of discrete pyrite grains associated with organic matter. Note large anhedral crystal of apatite (Ap) as well as muscovite (Ms), biotite (Bt), and quartz (Qtz). The finer-grained matrix consists of calcite, siderite (Sid), chlorite (Chl), and clay. *B*, Pyrite crystals (~2 micrometers in diameter) form a 60-micrometer mass rimming calcite (Cc) and organic matter (black). Note cellular structure of pyrite, suggesting that the pyrite has replaced organic matter.

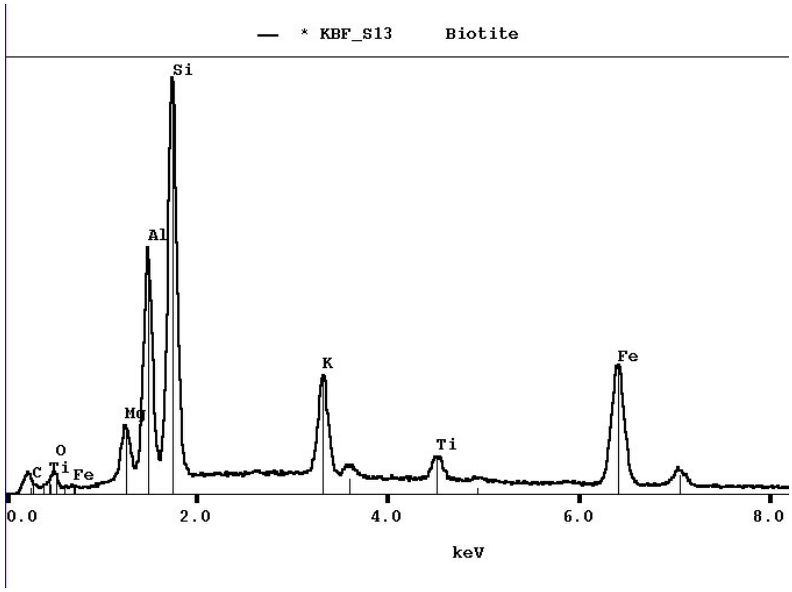

Figure 5.14. Kanawha Black Flint Shale (Sample KBF-WV). The representative EDS spectra show that the biotite is iron-rich, with minor amounts of titanium and magnesium.

Brush Creek Shale (Sample BCS3-PA). The Brush Creek shale is an ADTI reference standard selected as a primary rock sample for weathering experiments (Table 5.1). The shale has moderately high total sulfur (0.90 to 0.93 weight percent) and moderate NP values. Although the shale is classified as a "gray zone" sample for AMD predictions, it is associated with alkaline mine drainage throughout the bituminous coal region of Pennsylvania (Brady et al., 1998).

The Brush Creek Shale sample contained very little organic material based on whole-rock low-temperature ash (100 weight percent) and loss-on-ignition (12 weight percent LOI). Many of the rock chips were fossil-rich; some contain inclusions of calcite or barite (Figures 5.15 and 5.16). Some rock chips show a prominent rock fabric, with elongated mineral grains and black inclusions that contain variable amounts of organic material and pyrite framboids (Figure 5.17). Pyrite framboids had complex internal structures composed of individual pyrite grains ranging from <1 micrometer to 10 micrometers or more (Figure 5.18).

The mineralogical composition of the shale (in weight percent) is: 34 % quartz, 37% micas and clay minerals, 11% chlorite, 2% feldspar, 3% pyrite, and 10% carbonate minerals (Table 5.4). The carbonate minerals include calcite, ankerite, and siderite. Although the carbonate minerals are a minor component of the rock, the XRD pattern for siderite is distinct from that of calcite or ankerite/dolomite. Three separate samples of the composite shale were analyzed by XRD to examine shale heterogeneity and reproducibility of quantitative XRD results. Statistical errors associated with the Rietveld refinement of each pattern are represented by the error of fit (Table 5.5); errors associated with each mineral are $\pm$ 1.4 weight percent or less. The spread in estimates indicates sample heterogeneity as well as systematic errors in sample preparation and XRD methodology.

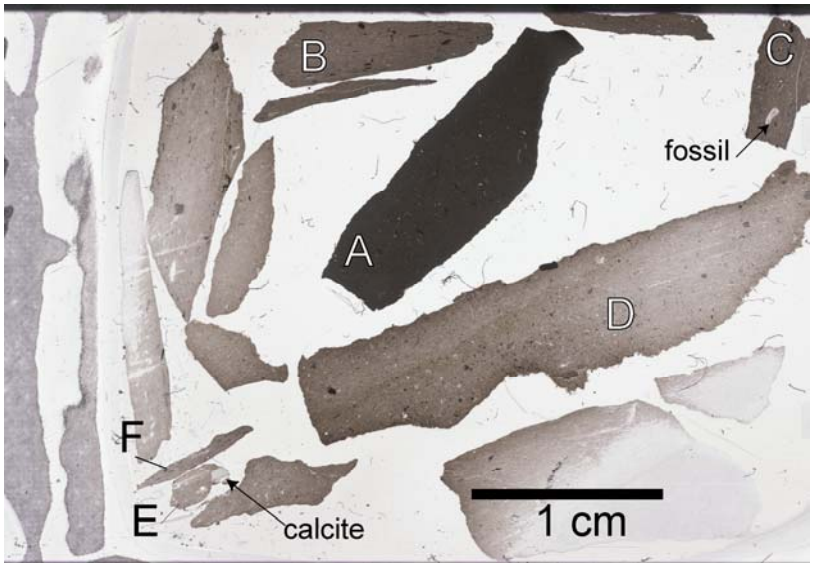

Figure 5.15. Brush Creek Shale (Sample BCS3-PA). Scanned image of polished thin section. Note calcite along the edge of chip E; fossil in chip C.

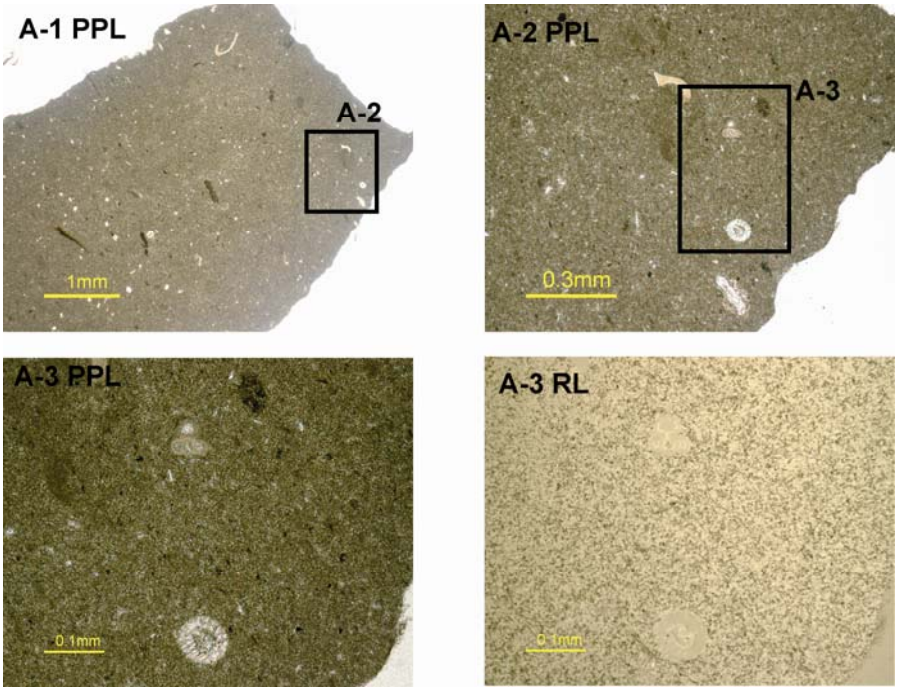

Figure 5.16. Brush Creek Shale (Sample BCS3-PA). Photomicrographs of rock fragment A showing shale textures at successively higher magnification. The shale consists of 0.5 millimeters calcite fossil fragments and elongated dark-colored clots of organic material, pyrite, and clay set in a fine-grained groundmass mainly composed of quartz, chlorite, calcite, siderite, and clay. The groundmass grain size is less than 20 micrometers. PPL, plane-polarized light. RL, reflected light.

Table 5.5. Mineralogy for BCS-3 on replicate splits of raw leach column starting material.

	Split 1		Split 2		Split 3	
Chi^2	3.8		5.5		5.6	
Phase	Weight%	±	Weight%	±	Weight%	±
Quartz	34.4	*1.0*	31.5	*1.0*	30.4	*0.6*
Chlorite	10.9	*0.5*	9.4	*0.5*	9.9	*0.4*
Muscovite	16.8	*0.7*	25.9	*1.4*	21.3	*0.9*
Phengite	6.8	*1.1*	8.3	*1.4*	4.3	*0.5*
Illite	8.6	*0.9*	5.3	*0.8*	10.0	*0.5*
Kaolinite	5.2	*0.4*	6.2	*0.3*	4.0	*0.2*
Micas & clay	37.4		45.7		39.6	
Albite	0.0		0.0		0.0	
Anorthite	0.2	*1.3*	0.4	*1.1*	3.4	*0.9*
Orthoclase	1.6	*0.8*	1.0	*0.7*	0.0	*0.6*
Feldspars	1.8		1.4		3.4	
Apatite	0.0		1.2	*0.6*	2.3	*0.4*
Zircon	0.9	*0.2*	1.0	*0.2*	0.3	*0.1*
Rutile	0.7	*0.3*	1.3	*0.2*	1.4	*0.2*
Accessory minerals	1.6		3.5		4.0	
Gypsum	0.0		0.0		0.0	
Barite	0.9		0.5	*0.2*	0.0	
Pyrite	3.0	*0.3*	3.6	*0.2*	2.7	*0.2*
Calcite	2.9	*0.3*	1.2	*0.1*	2.3	*0.3*
Siderite	4.7	*0.3*	3.3	*0.3*	7.0	*0.5*
Ankerite	2.4	*0.4*	0.0		0.8	*0.3*
Carbonate minerals	10.0		4.5		10.0	

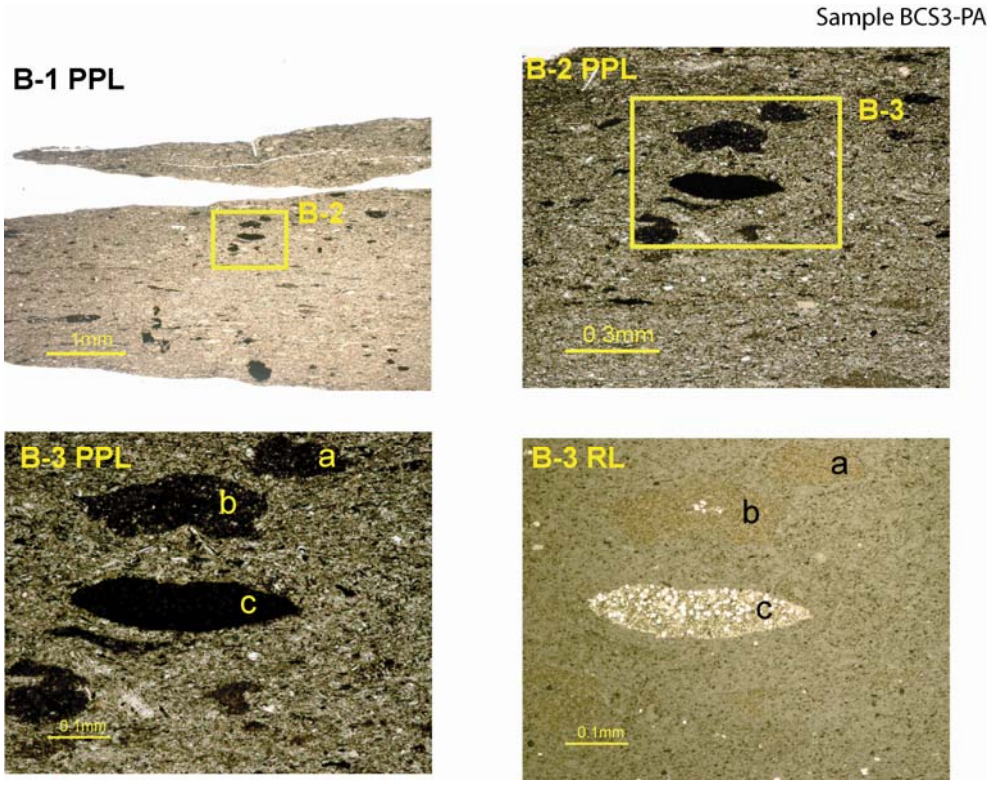

Figure 5.17. Brush Creek Shale (Sample BCS3-PA). Photomicrographs of rock fragment B showing details of elongated, dark brown to black clots. Reflected light (RL) microscopy shows that pyrite (bright white) is present as tiny disseminated grains in the shale matrix and as framboid fillings and cores within the black clots. Comparison of area B-3 at the same magnification in plane and reflected light shows the variation in clot composition from pyrite-free (a), to pyrite-cored (b), to pyrite-filled (c).

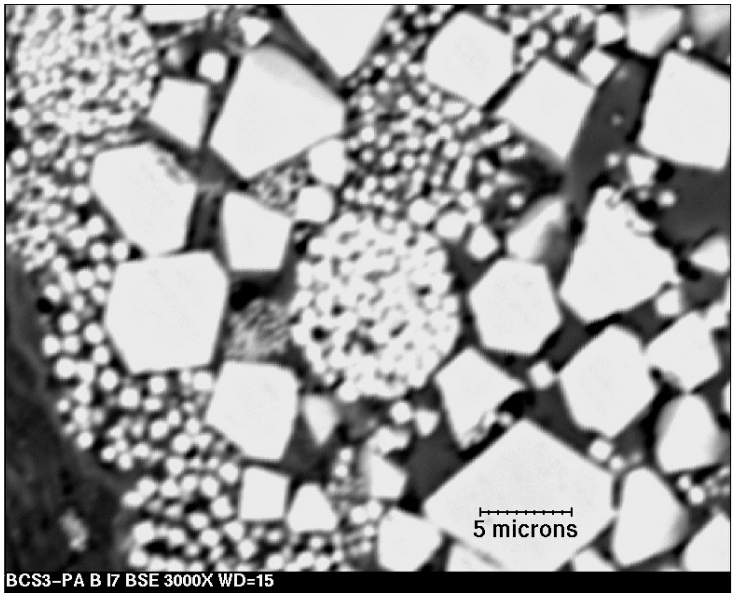

Figure 5.18. Brush Creek Shale (Sample BCS3-PA). SEM image (3,000X) of a pyrite framboid.

SEM data show that fossils are calcite with minor iron and manganese. Groundmass carbonates are zoned with calcic cores and more iron-rich rims. The zoning is apparent in backscattered SEM images because the iron-rims appear brighter due to average atomic number contrasts with more calcic cores (Figure 5.19).

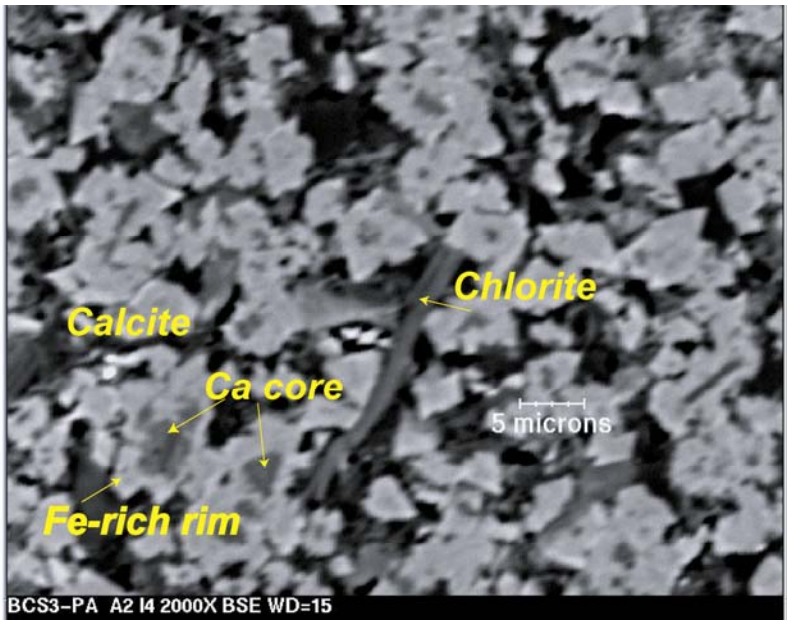

Figure 5.19. Brush Creek Shale (Sample BCS3-PA). SEM image (2,000X) of a groundmass carbonates. Much of the calcite is zoned, with calcium-rich cores (dark gray) surrounded by iron-rich rims (whiter areas).

Middle Kittanning Sandstone (Sample MKSS). The Middle Kittanning Sandstone sample was collected from Hawbaker quarry in Clearfield County, PA. The sandstone has low NP and low total sulfur (0.09 weight percent). MKSS was included as a relatively inert sample and was expected to behave as a minimal contributor of target analytes in the leaching study. Sample MKSS had a low temperature ash measurement of 91 weight percent and a loss-on-ignition of 5 weight percent. MKSS is a homogeneous, quartzose sandstone having an equigranular texture (Figure 5.20). Angular to subrounded 0.3 millimeter quartz grains are cemented by a fine-grained groundmass of mica, chlorite, clay and carbonate (Figure 5.21). XRD analysis estimated the mineralogical composition (in weight percent) as: 65 % quartz, 18% micas and clay minerals, 4% chlorite, 2% feldspar, <1% pyrite, and 8% carbonate minerals (Table 5.4). The accessory minerals zircon, rutile, monazite, and apatite were all confirmed by SEM. MKSS contains zoned carbonate (Figure 5.21) as well as discrete, adjacent grains of calcite and siderite (Figure 5.22) near pyrite framboids. SEM analyses confirm the XRD analysis of kaolin.

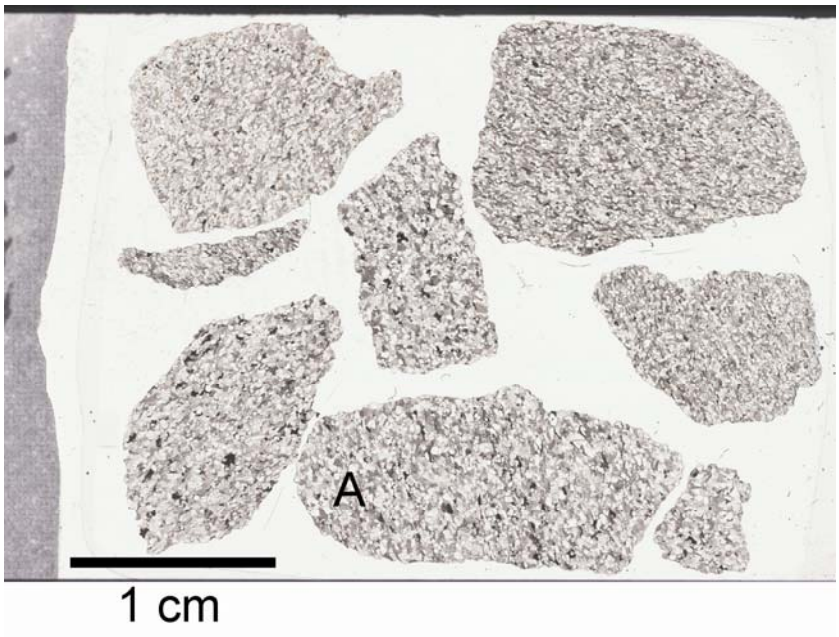

Figure 5.20. Middle Kittanning Sandstone (Sample MKSS). Scanned image of polished thin section. Note homogeneous texture of this rock.

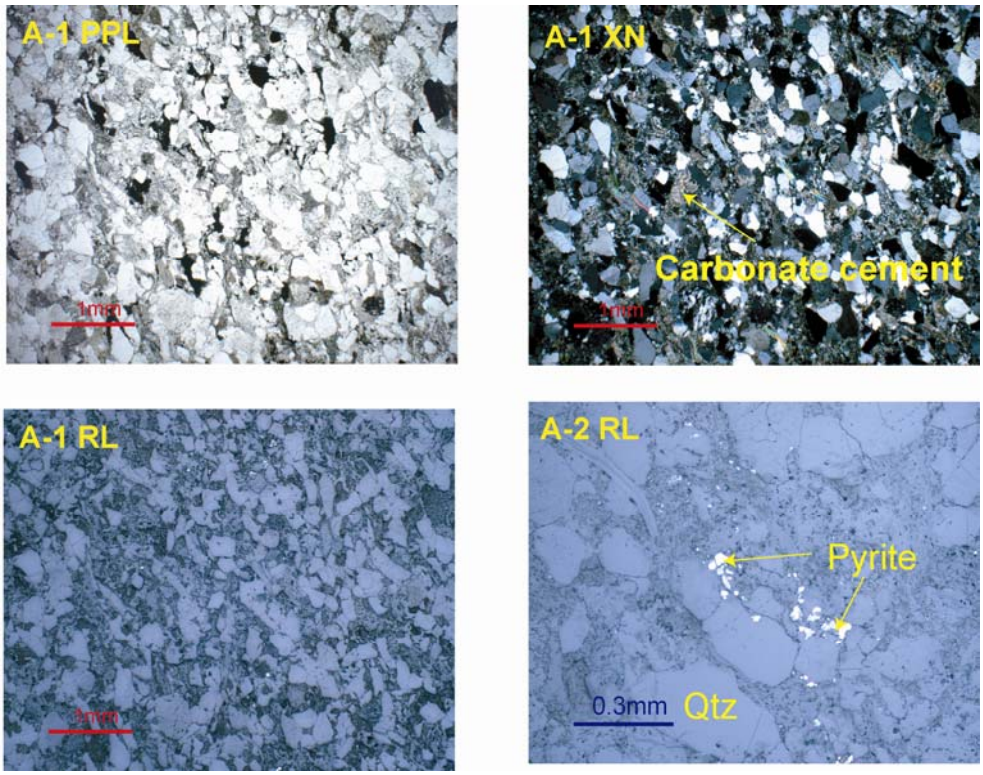

Figure 5.21. Middle Kittanning Sandstone (Sample MKSS). Photomicrographs of rock fragment A in plane light (PPL), crossed nicols (XN) view shows carbonate cementing millimeters-size quartz grains. Reflected light (RL) microscopy of same view (RL). A-2 RL, at higher magnification shows pyrite.

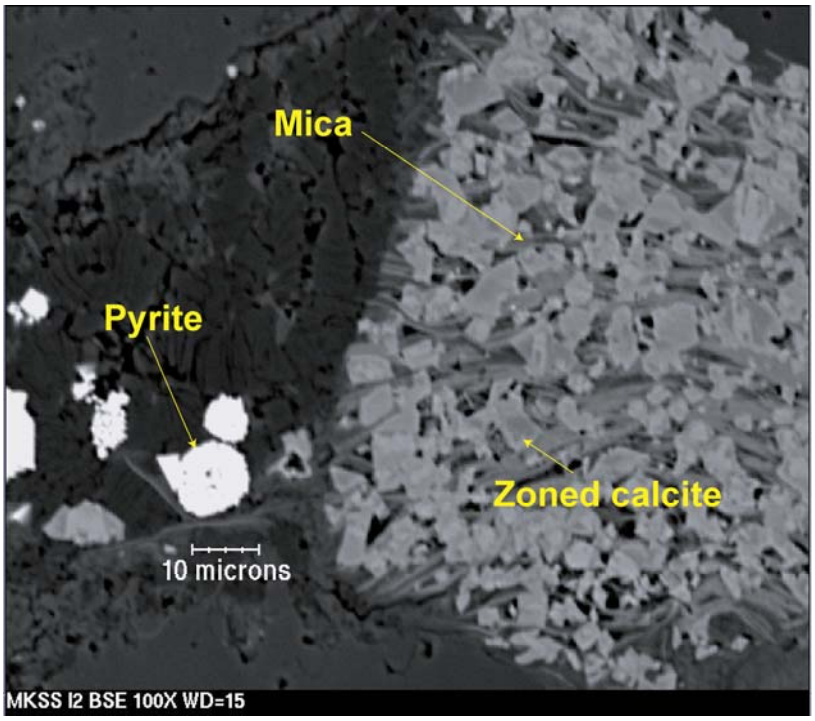

Figure 5.22. Middle Kittanning Sandstone (Sample MKSS). SEM image shows round clusters of pyrite framboids (bright white) and a large inclusion of zoned calcite and mica.

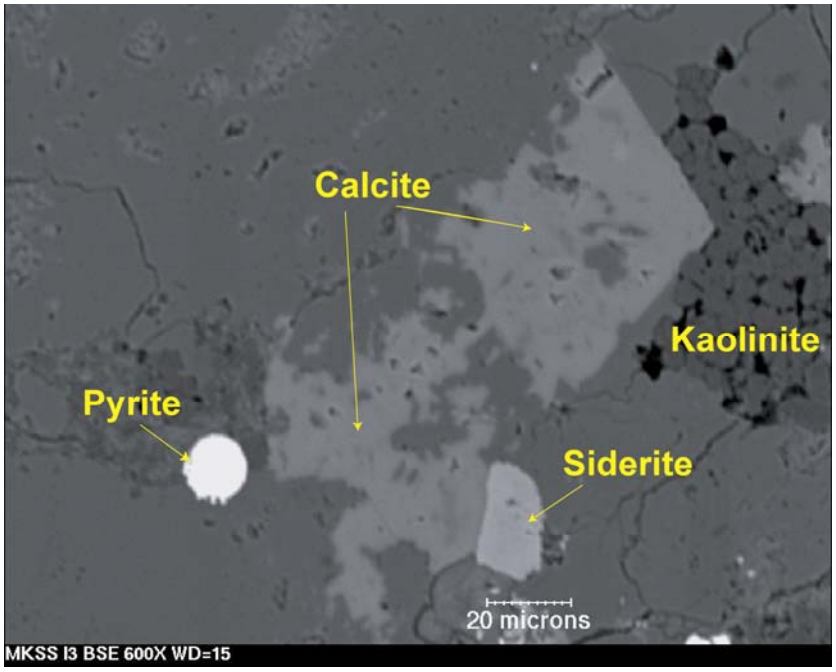

Figure 5.23. Middle Kittanning Sandstone (Sample MKSS). SEM image shows adjacent calcite and siderite near a round pyrite framboid and a clot of kaolinite.

Wadesville Sandstone (Sample Wadesville #29). Wadesville sandstone was selected as a secondary protocol standard because it has physical and chemical characteristics in marked contrast to the primary standard, the friable "gray-zone" Brush Creek Shale. The Wadesville is a calcareous sandstone that forms a hard lithologic unit (Hornberger et al., 2003). The sample was collected from a large open-pit surface anthracite mine in Schuylkill County, PA, where the mine pool discharge is one of the most alkaline natural discharges in the state of Pennsylvania (alkalinity >400 mg/L). The sample had negligible total sulfur (<0.1 weight percent) and significant NP (255 to 282 ppt). The Wadesville contained significantly more calcium (11.23 weight percent CaO), more carbon dioxide (16.2 weight percent CO_2), and less total sulfur (<0.02 weight percent) than any of the other samples included in this study (Table 5.2). In thin section, the sandstone was homogeneous from chip to chip (Figure 5.24). Coarse-grained carbonate cemented quartz grains; pyrite was sparse (Figure 5.25). XRD analysis estimated the mineralogical composition (in weight percent) as: 42 % quartz, 9% micas and clay minerals, 4% chlorite, 4% feldspar, <1% pyrite, and 38% carbonate minerals (Table 5.4).The low temperature ash treatment produced no mass loss. The sandstone also had the lowest estimated content of amorphous material (15 weight percent). No organic material was observed. SEM images and compositions confirm that the dominant carbonate mineral in the sample is zoned ankerite (Figure 5.26), in agreement with the XRD data. The outermost rims of each carbonate grain are iron-rich relative to the interior parts of the grain.

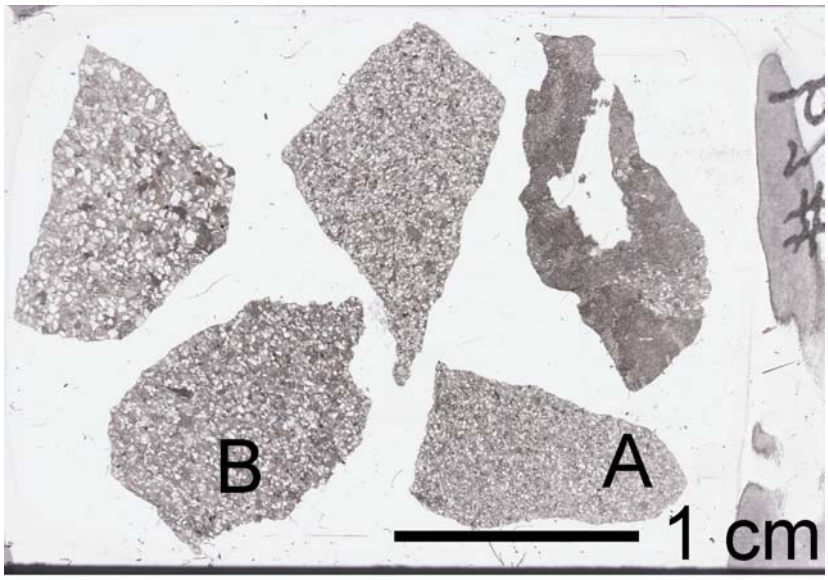

Figure 5.24. Wadesville Sandstone. Scanned image of polished thin section. Note homogeneous texture of this rock.

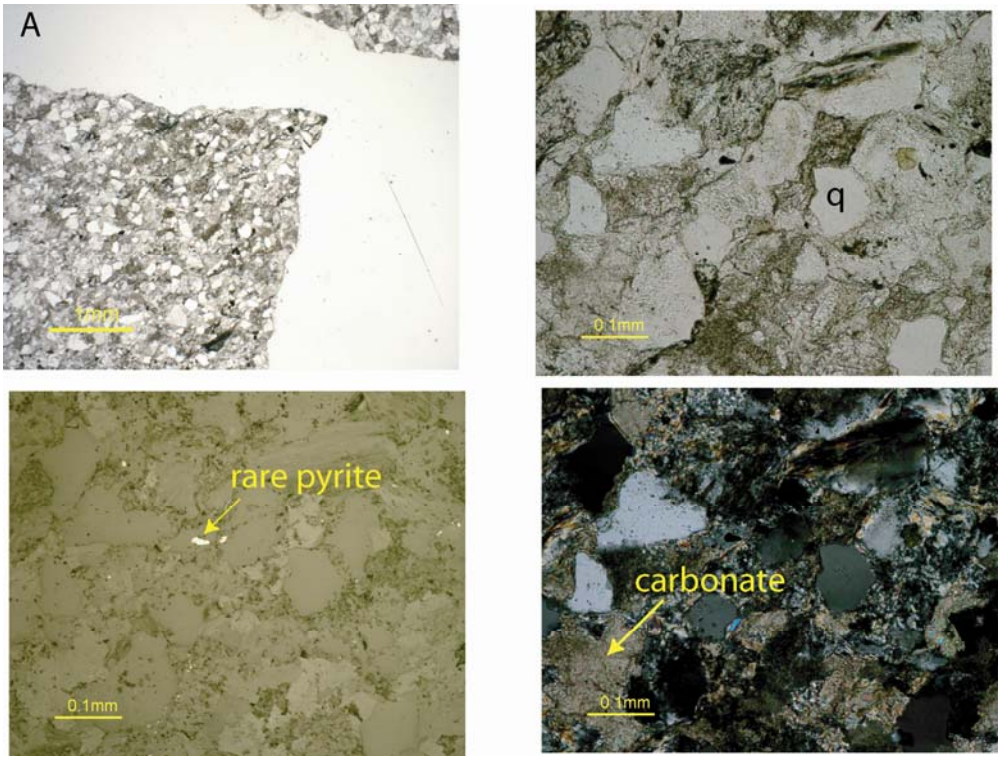

Figure 5.25. Wadesville Sandstone. Photomicrographs of rock fragment A in plane light (PPL) at low magnification (upper left). At higher magnification in plane, reflected light, and crossed nicols show quartz (q), rare pyrite, and the carbonate matrix (same view for all 3 photos).

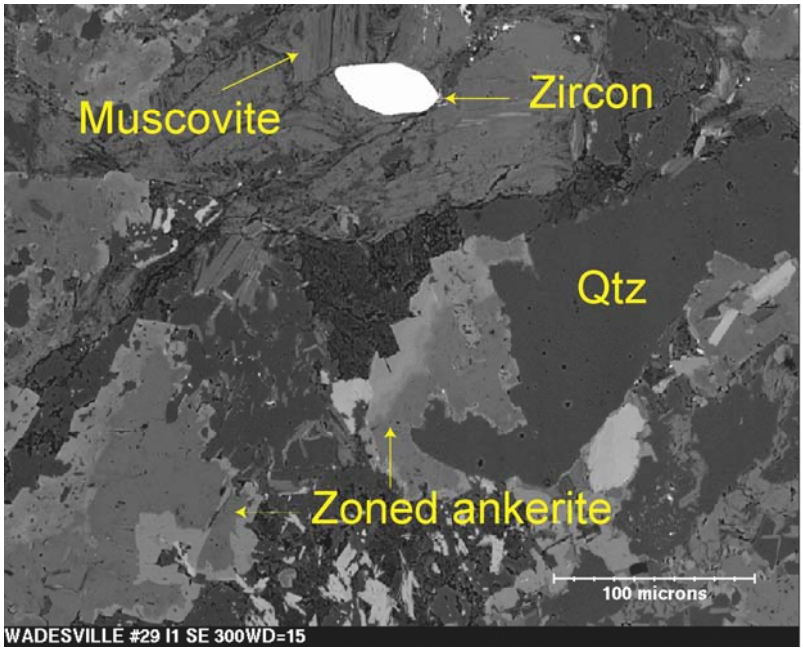

Figure 5.26. Wadesville Sandstone. SEM image of zoned carbonate cement in rock chip A. Note large zircon crystal in field of view.

Leechburg Coal Refuse (Sample LRBT#2). The Leechburg coal refuse deposits in Armstrong County, PA are associated with mines developed on the Lower Kittanning coal (Hornberger et al., 2005). The coal refuse was used in 2002 and 2003 weathering tests because of its high total sulfur content and low NP. The sample provided for characterization contains significant amounts of organic material, as indicated by the low-temperature ash determination (45 weight percent), significant amorphous content (77 weight percent), and significant volatile content (LOI 60 weight percent). The sample analyzed for geochemistry contained 5.5 weight percent total sulfur, 56 parts per million arsenic, and 952 parts per billion mercury (Table 5.2). XRD analysis estimated the mineralogical composition of the crystalline part of the material (in weight percent) as: 23 % quartz, 33% micas and clay minerals, 2% chlorite, 4% feldspar, 29% pyrite, and 2% carbonate minerals (Table 5.4). The sample was difficult to polish due to the high organic content, resulting in a smeared thin section (Figure 5.27). SEM images showed that the quartz grains were on the order of 5 micrometers in diameter. Although the pyrites were readily identifiable by SEM due to atomic number contrast with the quartz and organic material, they were too small to work with for determining mineral composition (Figure 5.28).

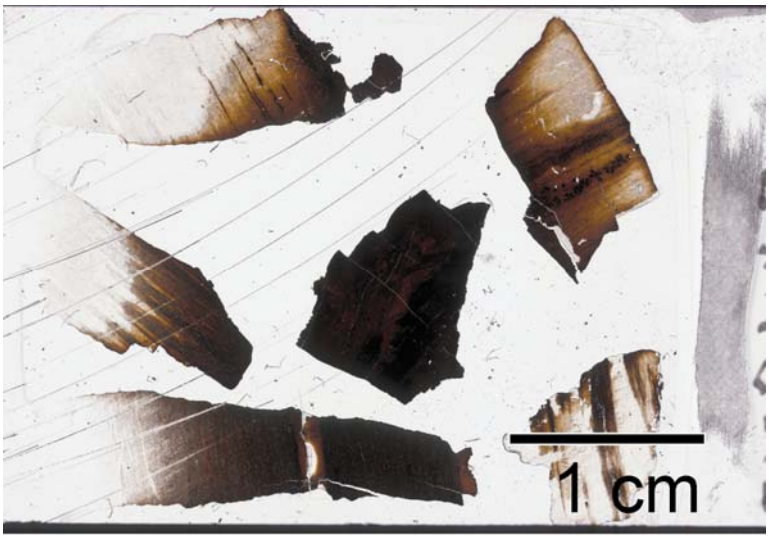

Figure 5.27. Leechburg Coal Refuse (Sample LRBT#2). Scanned image of a polished thin section. The sample is of organic material which complicated sample preparation and resulted in a thin, smeared mount.

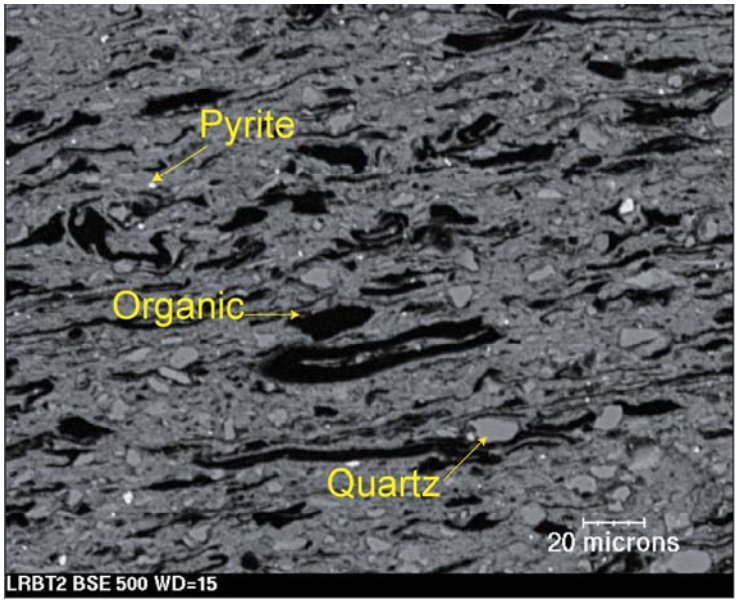

Figure 5.28. Leechburg Coal Refuse (Sample LRBT#2). SEM image showing fine-grained texture. The black material is organic; the bright white pinpoints are pyrite.

Mineral chemistry

Electron microprobe analytical data for pyrite and carbonate minerals are tabulated in Appendix 5.1, along with detection limits and statistics for each sample. Both mineral groups posed analytical challenges due to the fine grain size of the minerals. Ideally, mineral compositions total 100 (98 to 102) weight percent and computed atomic ratios match the expected mineral formulas. For pyrite, FeS_2, this means 2 atoms of sulfur for every atom of iron. Because the electron beam activates a volume of material at the mineral surface, uneven surfaces, holes, and the tiny grain size of individual pyrite grains in framboids produce low element totals. The atomic ratios, however, are appropriate for pyrite.

Pyrite. Pyrite was analyzed for iron, sulfur, selenium, nickel, arsenic, manganese, zinc, cadmium, cobalt, and copper. Trace element concentrations in pyrite varied within each sample; however, a few trends in the data are apparent (Figure 5.29). HCS-IN and Wadesville #29 were the only samples that contained selenium above detection limits; some pyrite in these samples contain over 1 weight percent manganese. Some pyrite grains in each sample contained arsenic above detection limits. Concentrations of other metals that typically occur in pyrite were at or below detection limits. Mercury was analyzed for in some samples, but none was detected. The trace elements are not evenly distributed throughout individual crystals in framboids, as shown by element maps (Figure 5.30). On these maps, the hotter colors indicate higher concentrations of an element. Note that the pyrite is outlined by high concentrations of iron, sulfur, arsenic, manganese, and selenium. The distribution of the trace elements is uneven across the pyrite crystals suggesting some zoning, even though spot analyses for selenium in pyrites in LKFC-WV are all below detection limits (Appendix 5.1) and the selenium concentrations in the bulk rock was <3 parts per million (Table 5.2). Sample HCS-IN has the highest whole-rock selenium content (81 parts per million; selenium was detected in 13 of the 17 pyrites analyzed from HCS-IN (Appendix 5.1).

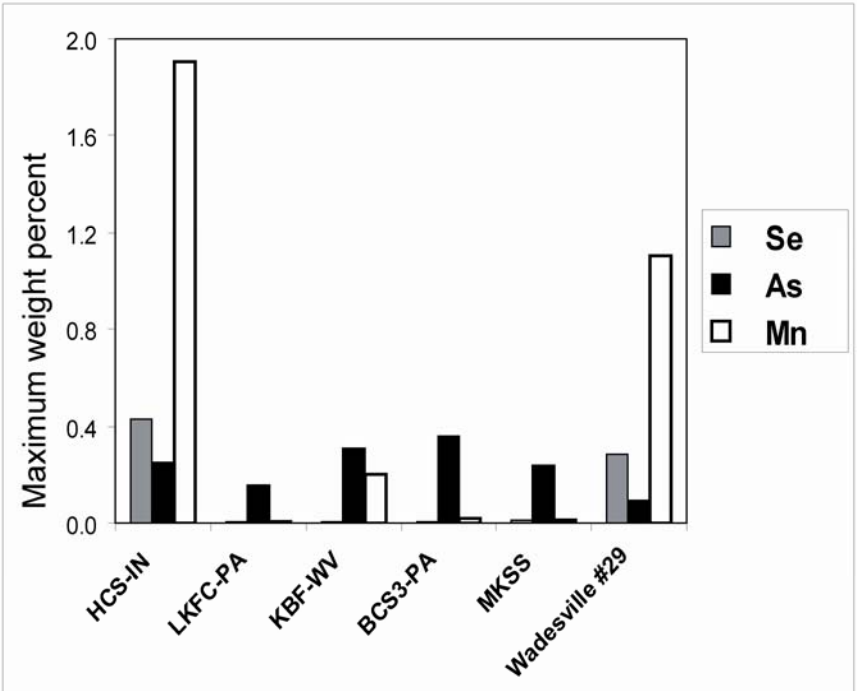

Figure 5.29. Trace elements in pyrite. The bar chart shows the maximum concentration of arsenic, selenium, and manganese detected in pyrite in each sample (Appendix 5.1)

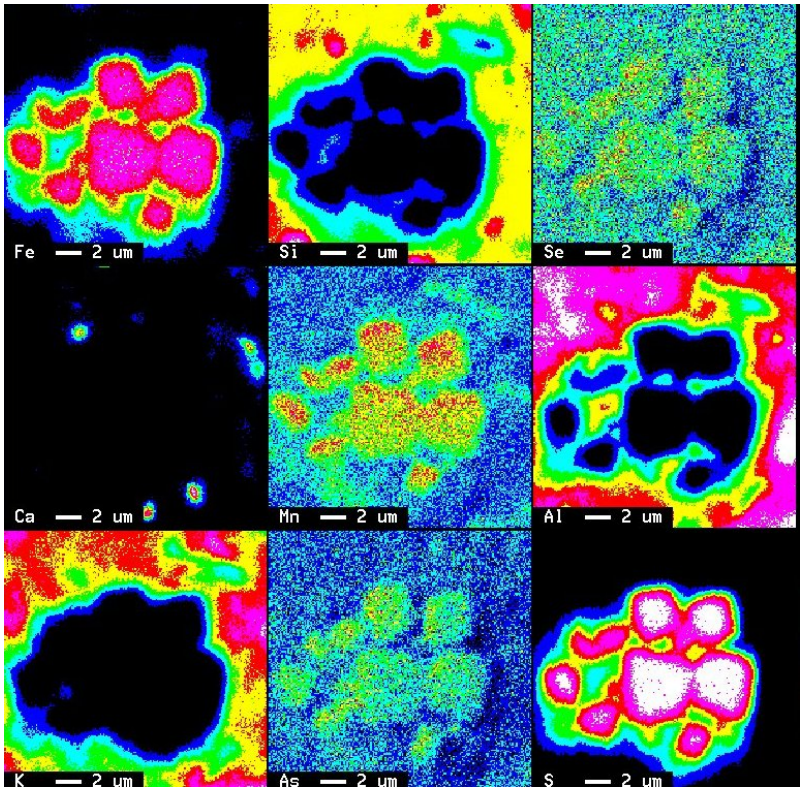

Figure 5.30. Trace elements in pyrite. The map shows the distribution of nine elements in and around a pyrite framboid in sample LKFC-PA.

Carbonate Minerals. Carbonate minerals are an analytical challenge because they tend to "cook" when exposed to an electron beam and because carbon is not analyzed. Typically, carbonates are analyzed by EPMA using a defocused (wide) electron beam. However, because of the zoning observed in carbonates in the SEM studies and the small grain size of minerals in shales, a focused beam was used for the analyses of both standards and unknowns. The elements calcium, magnesium, manganese, iron, and strontium were analyzed using carbonate minerals as standards, and the CO_2 content is calculated based on mineral stoichiometry ($CaCO_3$ for calcite, $FeCO_3$ for siderite, and $CaMg(CO_3)_2$ for dolomite group minerals. Silicon, aluminum, sodium, and potassium were analyzed as part of the carbonate mineral analysis package to screen for contaminants. Carbonate mineral analyses are tabulated in Appendix 5.1 by lithology, along with calculated CO_2 content and mineral formulas. Molar compositions are plotted in Figure 5.31, which is intended to illustrate the range of observed compositions of carbonate group minerals in the samples. Carbonate minerals in the leach column starting materials include calcite, siderite, and ankerite (ferroan dolomite). No pure dolomite compositions were observed (Figure 5.31). Quantitative XRD mineralogy for Houchin Creek Shale estimated about 3 weight percent carbonate minerals (Table 5.4). Localized patches of calcite in one of the rock chips (Figure 5.3A) were the only carbonate minerals observed in the thin section. The calcite contains about 0.5 weight percent MgO, 1.5 to weight percent MnO, and <1 weight percent FeO, and plots near the calcite apex on Figure 5.31. The Lower Kittanning Shale contains magnesian calcite in fossil fragments (Figure 5.10) and siderite in groundmass carbonate. The carbonate in Kanawha Black Flint Shale includes iron-rich ankerite and siderite with variable manganese (up to 6 weight percent MnO); calcite was also identified by SEM in contact with pyrite (Figure 5.13). In Brush Creek Shale, calcite occurs in shell fragments (Figure 5.16) and as zoned calcite in groundmass (Figure 5.19). Calcite cores are nearly pure; rims contain up to about 8 weight percent MnO + MgO + FeO. The Brush Creek calcite contains up to 0.5 weight percent SrO. Middle Kittanning Sandstone contains both siderite and calcite (Figures 5.22 and 5.23). Most of the microprobe data indicate magnesian siderite (up to 10 weight percent MgO, 1-2 weight percent MnO, <2 weight percent CaO); one analysis plotted in the ankerite field and three analyses indicate calcite with ~1 weight percent FeO, as much as 2 weight percent MnO, and traces of MgO. No siderite was detected in Wadesville Sandstone; all of the carbonate analyzed as ankerite or calcite (Figure 5.31).

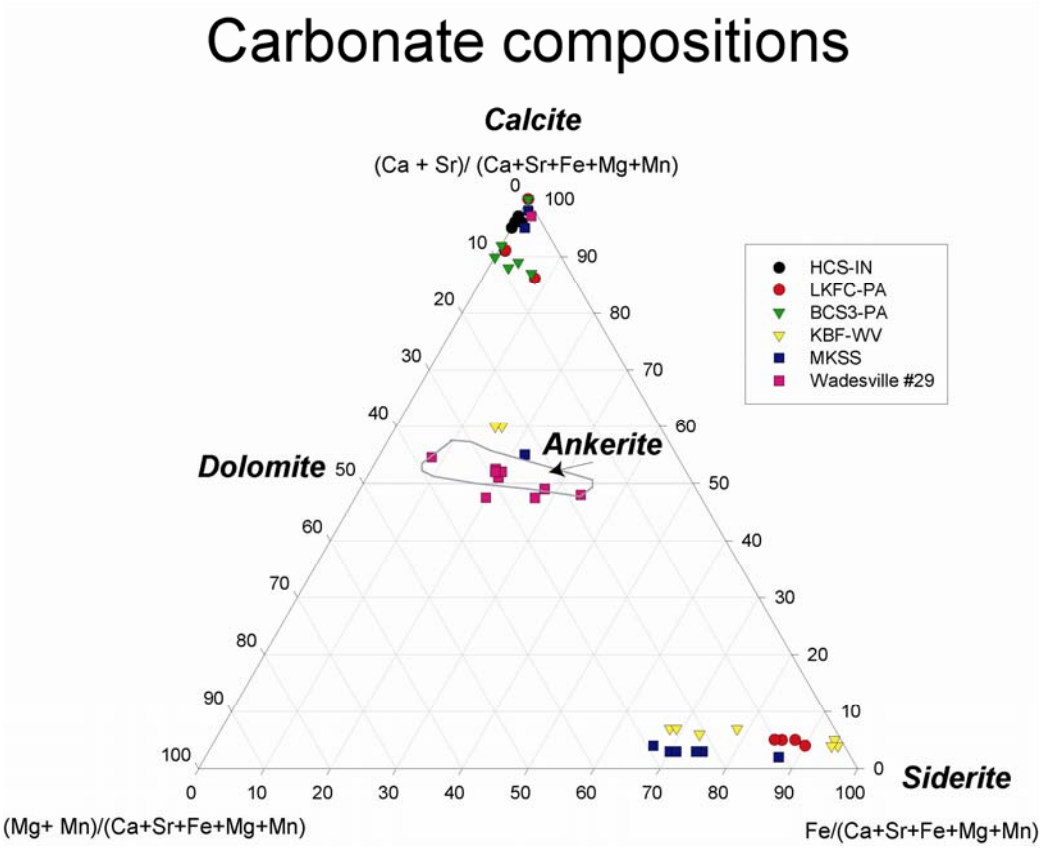

Figure 5.31. Carbonate mineral compositions. Molar cation ratios based on data in Appendix 5.1. The ankerite field is based on the compositional ranges for ankerites cited by Chang et al. (1996).

Leach column residues

Several months elapsed between the end of the leaching experiments and opening the columns. Thus, any minerals that were near-saturation in the final water column may have evaporated and precipitated, which complicates interpretation of weathering products. Residues differ in color from the starting material. The raw Houchin Creek Shale, for example, is black but the leach column residue material has a brownish-orange caste and some rock chips were partially coated with iron precipitates (Figure 5.32).

Carbon and sulfur analyses for leach column residues are listed in Table 5.2. Pre-and post leach total sulfur analyses are generally comparable or indicate an increase, and might reflect sample heterogeneity or analytical error. Quantitative XRD analyses of the leach column residues for HCS-IN (see LCR columns in Table 5.4) suggest that gypsum may have precipitated. The raw and LCR gypsum estimates for HCS-IN are 6.4 and 9.1 weight percent, respectively. The carbon species were determined for the LCR samples; these data indicate that CO_2 apparently decreased for HCS-IN and KBF-WV, but increased for the other samples. All of the shales contain graphite and organic carbon in the leach column residue. Carbon species were not determined for the raw material. The "before leaching" (raw and LTA) and "post-leaching" (LCR) XRD data suggest an apparent decrease in carbonate minerals for samples HCS-IN and BCS-3 and an apparent decrease in pyrite for samples HCS-IN and LKFC-PA. Paste pH measurements on leach column residues indicated that although the effluents from all columns at

week 16 were near-neutral, acid-generating weathering products accumulated in the columns for Houchin Creek Shale and possibly, for Lower Kittanning Shale (Figure 5.32*B*).

A

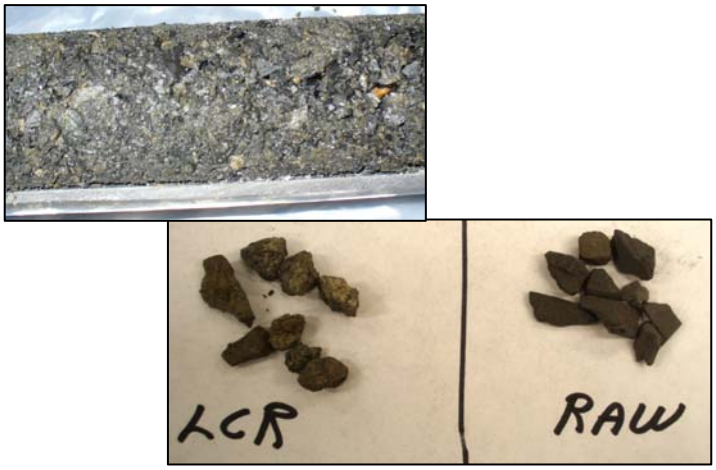

B

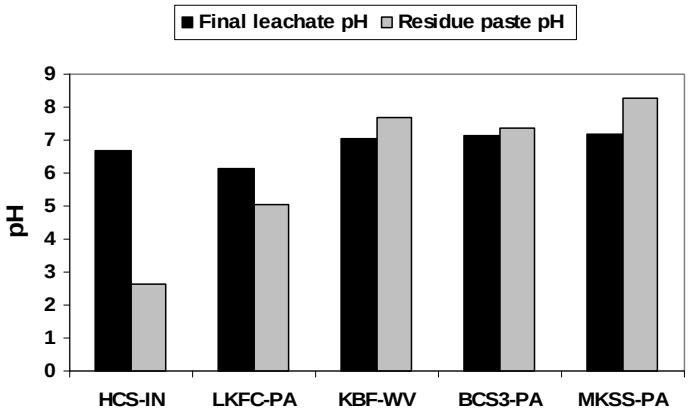

Figure 5.32. Leach columns were opened several months after the 16-week leach study was completed. *A*, Photographs of one of the Houchin Creek Shale columns. Rock chips from the leach column residue (LCR) show iron oxide coatings and precipitates that were not present in the black starting material (RAW). *B*, Comparison of final column effluent pH and paste pH on column residue material. Acid-generating weathering products accumulated in the HCS-IN column after the experiment ended.

Target analytes in leachates

In addition to monitoring pH, conductivity, alkalinity, and acidity, the laboratories that participated in this study analyzed dissolved concentrations of aluminum, calcium, iron, manganese, potassium, magnesium, selenium, zinc, and sulfate in column leachates. Data, evaluation, interpretation of results of the interlaboratory leaching study, effects of particle size, kinetic data, and implications for long-term weathering behavior are addressed elsewhere in this report. In this chapter, we include a series of graphs of data from one of the participating laboratories (USGS) as Appendices 5.2 and 5.3 as a framework for discussing mineralogical controls on leachate quality. Figures 5.33 through and 5.35 illustrate selected data from Appendices 5.2 and 5.3.

Despite an acid-base account based on total sulfur and neutralization potential that indicated potential for acidic effluent for two of the four shales, effluents from all of the columns were net alkaline with near-neutral pH at the end of the experiments. Figure 5.33 indicates that after the initial flush, leachate from all five rock samples was net alkaline based on hot acidity. The initial flush dissolved any weathering products that accumulated in the samples prior to onset of the weathering experiment. After the initial flush, alkalinity, pH, and calcium concentrations remained relatively stable. Figure 5.34 shows leachate concentrations for dissolved sulfate, calcium, iron, and aluminum over the course of the leaching study. Sulfate and calcium were detected in column effluent throughout the experiment; sulfate generally declines with time whereas calcium was relatively constant. After the first three weeks, iron and aluminum dropped off. The likely explanation for this behavior is the precipitation of iron and aluminum oxyhydroxide minerals due to hydrolysis reactions. Weathering of pyrite, siderite, or other iron-bearing minerals in the columns releases ferrous iron, which was readily oxidized to ferric iron under the oxidizing conditions of the experiment (effluent ORP $\geq$ 150 millivolts for all columns). For example, consider the reaction:

$$Fe^{3+}_{(dissolved)} + 3\ H_2O \rightarrow Fe(OH)_{3\ (Solid\ precipitate)} + 3H^+$$

These precipitates coated and cemented rock fragments in the leach column residue (Figure 5.32). Although the hydrolysis reactions generate acidity, sufficient alkalinity was present in the leach column material during the course of the experiment to consume the acid because the effluents remained net alkaline (Figure 5.33). See Appendix 5.2 for addition time-series data (concentration and cumulative transport graphs). Computations of saturation indices based on effluent chemistry using WATEQ4F (Ball and Nordstrom, 1991) indicate that with the exception of the initial flush, the effluents from all columns except those containing Lower Kittanning Shale (sample LKFC) were saturated or nearly saturated with calcite throughout the experiment (Figure 5.35A). Effluents from the Indiana shale HCS-IN were saturated or supersaturated with gypsum (Figure 5.35B), which is consistent with the apparent increase in gypsum detected by XRD for the leach column residue (Table 5.4). Precipitation of gypsum can potentially inhibit calcite dissolution. See Appendix 5.3 for computation of saturation indices.

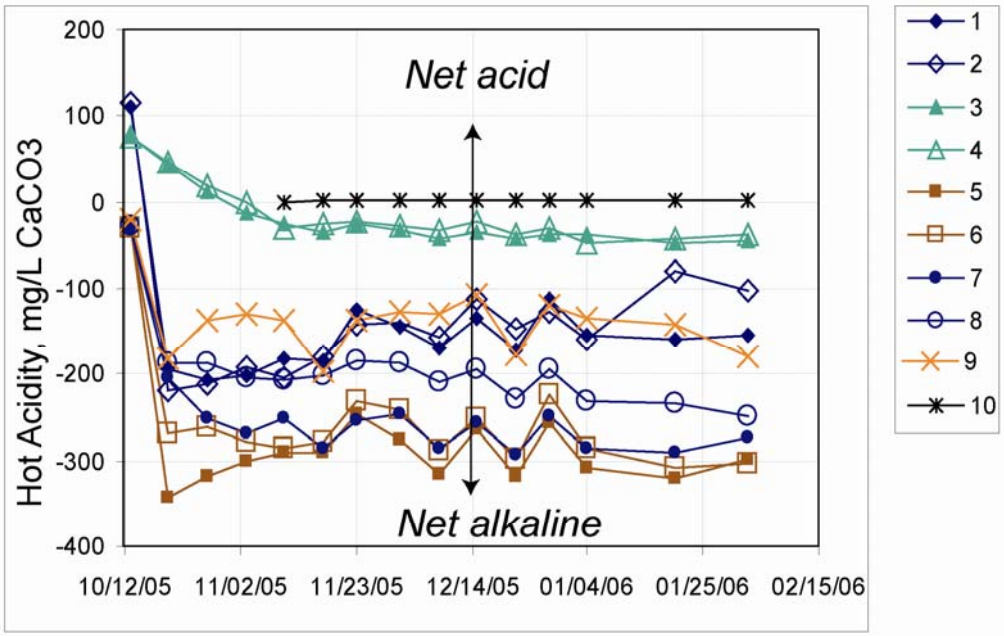

Figure 5.33. Hot acidity concentrations in leachates as a function of time for duplicate leach columns of Houchin Creek Shale (1 and 2), Lower Kittanning Shale (3 and 4), Kanawha Black Flint Shale (5 and 6), Brush Creek Shale (7 and 8), a single column of Middle Kittanning Sandstone (9), and deioinzed water (10). Hot acidity concentrations >0 indicate net acidity; hot acidity concentrations <0 indicate net alkalinity.

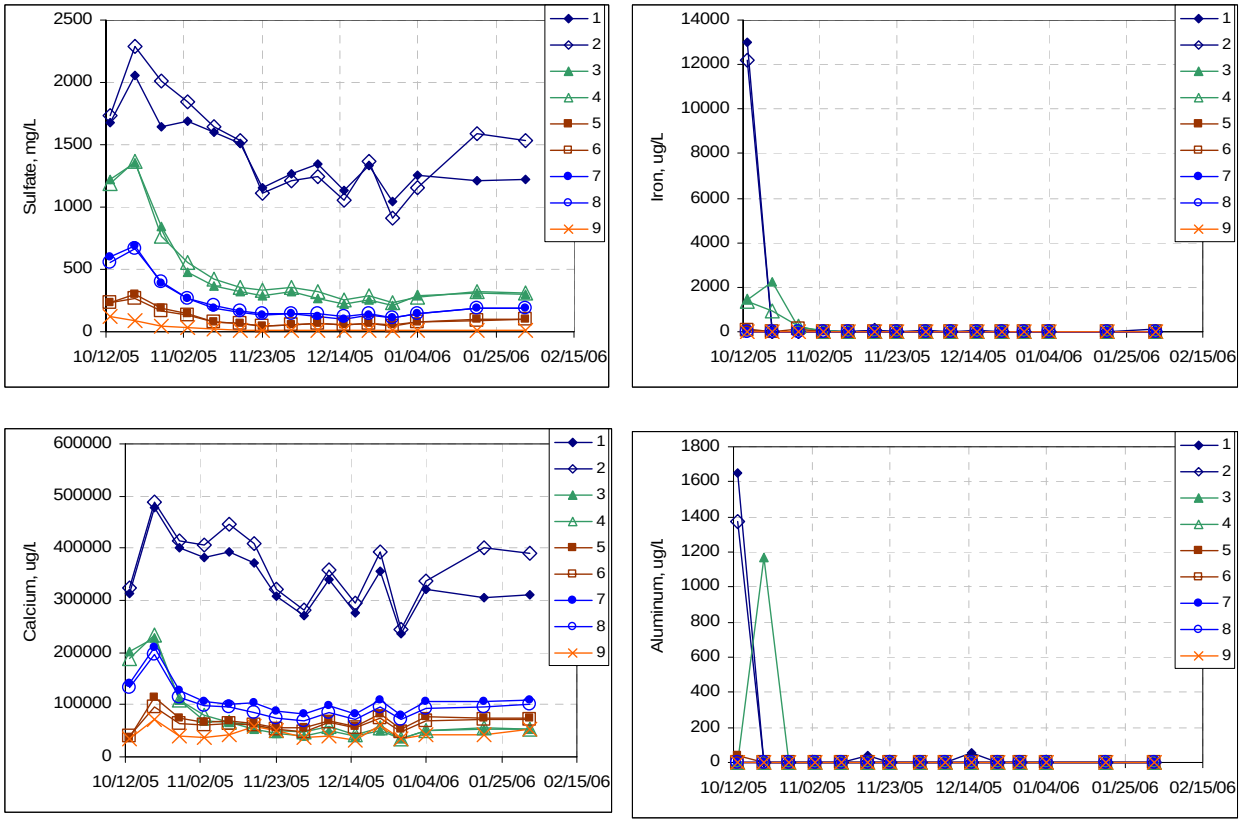

Figure 5.34. Concentrations of target analytes in leachates as a function of time for duplicate leach columns of Houchin Creek Shale (1 and 2), Lower Kittanning Shale (3 and 4), Kanawha Black Flint Shale (5 and 6), Brush Creek Shale (7 and 8), and a single column of Middle Kittanning Sandstone (9).

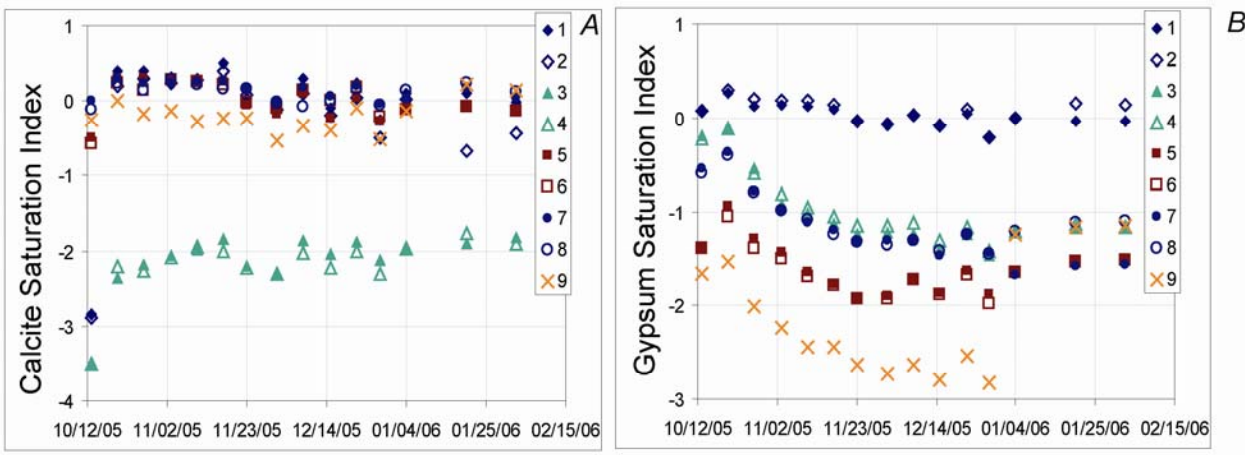

Figure 5.35. Effluent saturation indices for calcite (A) and gypsum (B). Saturation indices (log IAP/K) >0 indicate saturation or supersaturation of the solid phase. See Appendix 5.3 for details and references. Same sample key as Figure 5.34.

Trace elements in leachate

Rocks associated with coal beds may contain a variety of trace elements. The target analytes for the interlaboratory leachate tests included selenium and zinc. Because the geochemical data for the unweathered rocks in Table 5.2 showed variable concentrations of some other trace elements of potential environmental concern, we acquired a comprehensive element suite for the final leachates from one of the participating labs (Table 5.6). Effluent from duplicate columns was analyzed for all samples except KBF-WV; effluent from one column was analyzed for KBF-WV.

Zinc was the dominant base-metal in leachates (Table 5.6). Comparison of total base-metal concentrations in starting materials and leachates (Figure 5.36) indicates that the (1) duplicate columns produced similar base-metal leachate concentrations, (2) total base-metal concentration in leachates were < 10 mg/L for all samples, (3) Houchin Creek shale produced the highest concentrations of base metals in leachate. Although cadmium was below detection limits (0.5 parts per million) in the starting materials, the leachate data show that cadmium concentrations increase linearly with increasing effluent zinc (Figure 5.37). None of the effluents contained mercury above detection levels (6 nanograms per liter). Selenium was detected in concentrations of >5 micrograms per liter in effluent from the Houchin Creek, Lower Kittanning, and Brush Creek shales whereas the Kanawha Black Flint shale from West Virginia had the lowest selenium leachate concentration of all the samples (Figure 5.38). Other elements that can be released upon weathering of pyrite include arsenic and thallium, both of which were detected in all of the leachates.

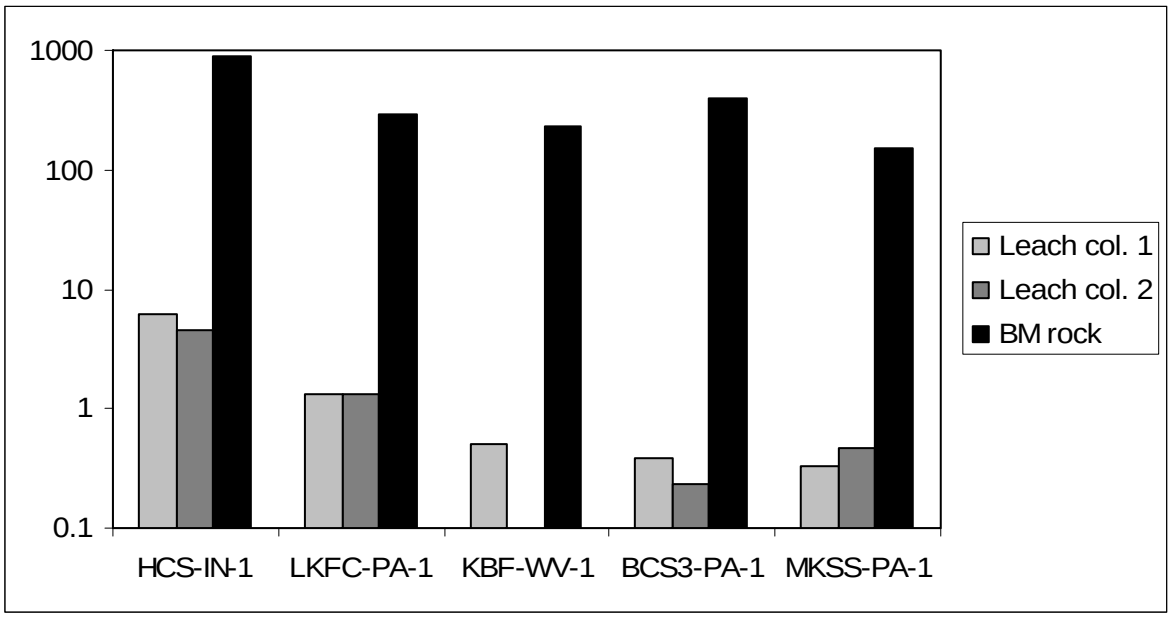

Figure 5.36. Base-metal concentrations in starting materials (BM rock) and leachates in parts per million and mg/L, respectively.

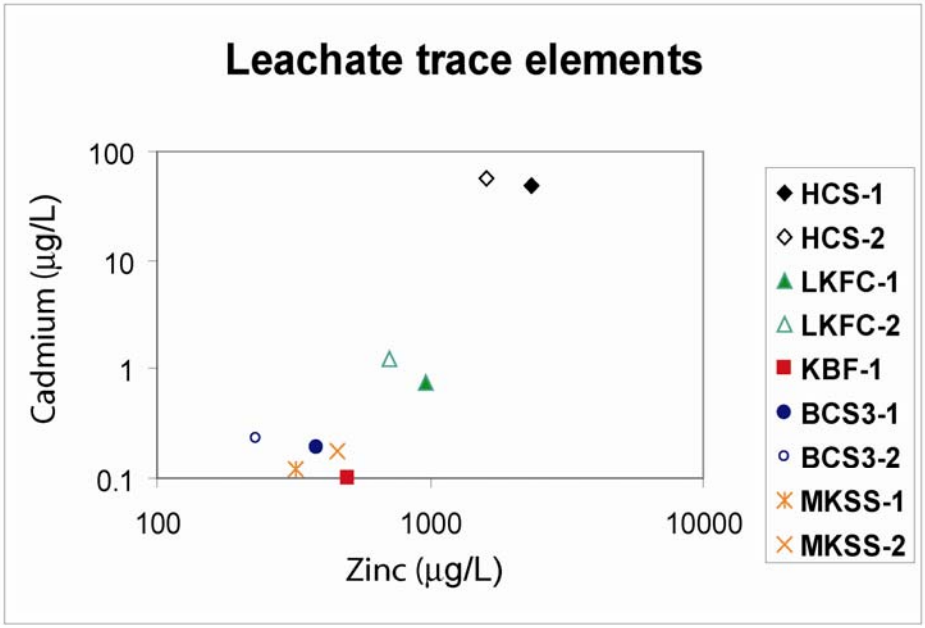

Figure 5.37. Cadmium and zinc in leach column effluent. Duplicate columns (1 and 2).

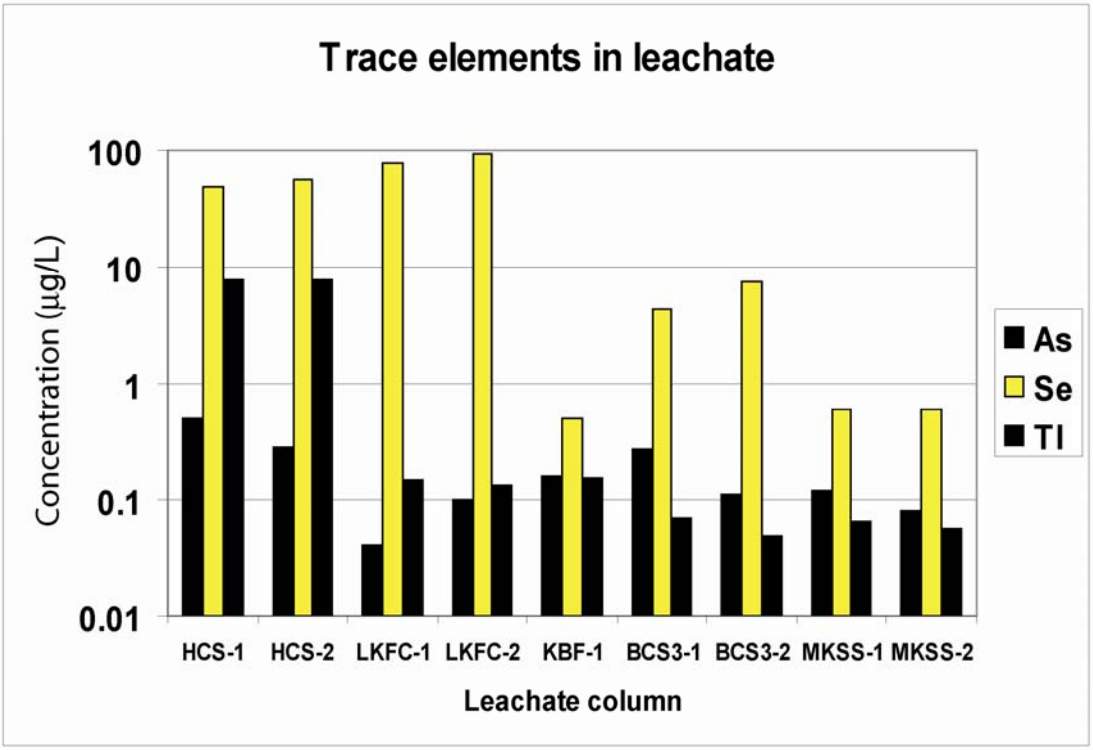

Figure 5.38. Trace elements in leachates.

Table 5.6. Trace elements in final leach column effluent from one laboratory.
[1 and 2 represent duplicate columns. Methods: MS, ICP-MS; OES, ICP-OES used when ICP-MS concentrations exceed upper limits of the method; FIMS for mercury. Element concentrations are reported in micrograms per liter (µg/L), milligrams per liter (mg/L), and (or) nanograms per liter (ng/L)]

Element		D.L.	Method	HCS-IN		LKFC-PA		KBF-WV	BCS3-PA		MKSS	
	units			1	2	1	2	1	1	2	1	2
Ag	µg/L	0.2	MS	< 0.2	< 0.2	< 0.2	< 0.2	< 0.2	< 0.2	< 0.2	< 0.2	< 0.2
Al	µg/L	2	MS	3	7	2	3	< 2	9	5	8	11
As	µg/L	0.03	MS	0.5	0.28	0.04	0.1	0.16	0.27	0.11	0.12	0.08
Au	µg/L	0.002	MS	0.003	< 0.002	< 0.002	< 0.002	< 0.002	< 0.002	< 0.002	< 0.002	< 0.002
Ba	µg/L	0.1	MS	25.7	26.6	54	68.5	106	70.8	65.5	66.4	75.3
Be	µg/L	0.1	MS	< 0.1	< 0.1	< 0.1	< 0.1	< 0.1	< 0.1	< 0.1	< 0.1	< 0.1
Bi	µg/L	0.3	MS	< 0.3	< 0.3	< 0.3	< 0.3	< 0.3	< 0.3	< 0.3	< 0.3	< 0.3
Br	µg/L	3	MS	192	190	230	228	235	202	132	168	162
Ca	µg/L	700	MS	> 20000	> 20000	> 20000	> 20000	> 20000	> 20000	> 20000	> 20000	> 20000
Ca	mg/L	0.1	OES	628	580	171	218	205	320	196	89.6	111
Cd	µg/L	0.01	MS	48.1	56.1	0.73	1.24	0.1	0.19	0.23	0.12	0.18
Ce	µg/L	0.001	MS	0.266	0.269	0.235	1.49	0.019	0.036	0.037	0.029	0.009
Co	µg/L	0.005	MS	> 200	194	70.8	122	0.277	1.43	0.048	1.41	1.79
Co	µg/L	2	OES	207	--	--	--	--	--	--	--	--
Cr	µg/L	0.5	MS	< 0.5	< 0.5	< 0.5	< 0.5	1.5	1.2	< 0.5	< 0.5	< 0.5
Cs	µg/L	0.001	MS	0.201	0.169	0.068	0.096	0.129	0.045	0.032	0.059	0.047
Cu	µg/L	0.2	MS	0.7	3.4	1.5	1.7	< 0.2	< 0.2	0.5	1.3	1.7
Dy	µg/L	0.001	MS	0.069	0.033	0.017	0.131	0.003	0.008	0.004	0.004	< 0.001
Er	µg/L	0.001	MS	0.048	0.019	0.01	0.061	0.003	0.007	0.002	0.003	0.001
Eu	µg/L	0.001	MS	0.009	0.005	0.006	0.03	0.01	0.006	0.003	0.006	0.003
Fe	µg/L	10	MS	< 10	< 10	< 10	< 10	< 10	< 10	< 10	< 10	10
Ga	µg/L	0.01	MS	0.14	0.16	0.47	0.62	< 0.01	0.04	< 0.01	0.03	0.03
Gd	µg/L	0.001	MS	0.063	0.04	0.021	0.211	0.004	0.007	0.004	0.005	0.001
Ge	µg/L	0.01	MS	0.26	0.28	0.31	0.37	0.03	0.03	0.05	0.04	0.02
Hf	µg/L	0.001	MS	0.002	0.003	< 0.001	0.002	0.007	0.006	< 0.001	0.002	< 0.001
Hg	µg/L	0.2	MS	< 0.2	< 0.2	< 0.2	< 0.2	< 0.2	< 0.2	< 0.2	< 0.2	< 0.2
Hg	ng/L	6	FIMS	< 6	< 6	< 6	< 6	< 6	< 6	< 6	< 6	< 6
Ho	µg/L	0.001	MS	0.017	0.009	0.003	0.029	< 0.001	0.002	0.001	< 0.001	< 0.001
I	µg/L	1	MS	41	81	68	99	17	31	10	130	18
In	µg/L	0.001	MS	< 0.001	< 0.001	< 0.001	< 0.001	< 0.001	< 0.001	< 0.001	< 0.001	< 0.001
K	µg/L	30	MS	5000	4780	9690	10800	18400	8000	6350	9120	7990
La	µg/L	0.001	MS	0.162	0.241	0.229	1.07	0.016	0.021	0.021	0.034	0.009
Li	µg/L	1	MS	131	140	57	76	59	24	16	11	11
Lu	µg/L	0.001	MS	0.005	0.001	< 0.001	0.003	< 0.001	< 0.001	< 0.001	< 0.001	< 0.001
Mg	µg/L	1	MS	> 20000	> 20000	> 20000	> 20000	> 20000	> 20000	> 20000	> 20000	> 20000
Mg	mg/L	0.1	OES	192	228	133	173	124	106	96.5	18.9	23.9
Mn	µg/L	0.1	MS	> 10000	> 10000	> 10000	> 10000	150	2500	8.6	1320	1410
Mn	mg/L	0.01	OES	11.6	10.6	42.8	43	--	--	--	--	--
Mo	µg/L	0.1	MS	101	54.5	0.1	0.3	0.2	0.6	0.9	0.4	0.4
Na	µg/L	5	MS	19400	21700	4810	6420	2200	8030	8290	1280	1520
Nb	µg/L	0.005	MS	0.015	0.011	< 0.005	< 0.005	0.007	0.015	0.006	< 0.005	< 0.005
Nd	µg/L	0.001	MS	0.164	0.111	0.068	0.52	0.009	0.022	0.013	0.028	0.006

				HCS-IN		LKFC-PA		KBF-WV	BCS3-PA		MKSS	
Ni	µg/L	0.3	MS	> 1000	> 1000	256	485	3.2	4.5	1.4	2.8	5.6
Ni	µg/L	5	OES	3550	2710	--	--	--	--	--	--	--
Os	µg/L	0.002	MS	< 0.002	< 0.002	< 0.002	< 0.002	< 0.002	< 0.002	< 0.002	< 0.002	< 0.002
Pb	µg/L	0.01	MS	0.91	4.33	0.22	0.33	0.27	0.17	0.51	0.3	0.3
Pd	µg/L	0.01	MS	< 0.01	< 0.01	0.03	0.02	0.03	0.13	0.03	0.02	0.01
Pr	µg/L	0.001	MS	0.035	0.027	0.017	0.13	0.003	0.005	0.004	0.006	< 0.001
Pt	µg/L	0.3	MS	< 0.3	< 0.3	< 0.3	< 0.3	< 0.3	< 0.3	< 0.3	< 0.3	< 0.3
Rb	µg/L	0.005	MS	12.2	11.2	13.7	15.1	30.8	5.12	4	6.75	6.35
Re	µg/L	0.001	MS	0.331	0.263	0.002	0.002	0.004	0.004	0.002	0.004	0.004
Ru	µg/L	0.01	MS	0.03	0.02	< 0.01	< 0.01	< 0.01	< 0.01	< 0.01	< 0.01	< 0.01
Sb	µg/L	0.01	MS	1.19	0.73	0.1	0.18	0.1	0.19	0.24	0.24	0.28
Sc	µg/L	1	MS	1	< 1	< 1	< 1	3	2	< 1	< 1	< 1
Se	µg/L	0.2	MS	48.8	56.9	79.1	93.1	0.5	4.3	7.6	0.6	0.6
Si	µg/L	200	MS	5300	3100	1900	2000	9400	7000	2100	1700	1300
Sm	µg/L	0.001	MS	0.035	0.017	0.009	0.103	0.003	0.002	0.002	0.004	< 0.001
Sn	µg/L	0.1	MS	0.7	2.1	0.8	2.8	1.2	2.1	6	3.6	1.8
Sr	µg/L	0.04	MS	> 200	> 200	> 200	> 200	> 200	> 200	> 200	129	149
Sr	µg/L	10	OES	1040	1080	450	550	2380	990	690	--	--
Ta	µg/L	0.001	MS	< 0.001	< 0.001	< 0.001	< 0.001	< 0.001	< 0.001	< 0.001	< 0.001	< 0.001
Tb	µg/L	0.001	MS	0.011	0.005	0.003	0.027	< 0.001	0.001	< 0.001	< 0.001	< 0.001
Te	µg/L	0.1	MS	< 0.1	< 0.1	< 0.1	< 0.1	< 0.1	< 0.1	< 0.1	< 0.1	< 0.1
Th	µg/L	0.001	MS	0.002	0.002	< 0.001	< 0.001	0.002	0.001	0.001	< 0.001	< 0.001
Ti	µg/L	0.1	MS	0.6	0.4	0.2	0.2	0.8	0.5	0.2	0.1	< 0.1
Tl	µg/L	0.001	MS	7.81	7.67	0.148	0.135	0.153	0.069	0.048	0.064	0.057
Tm	µg/L	0.001	MS	0.005	0.001	< 0.001	0.005	< 0.001	0.001	< 0.001	< 0.001	< 0.001
U	µg/L	0.001	MS	> 200	41.3	0.148	0.1	2.26	5.47	3.91	1.75	1.9
U	mg/L	0.05	OES	0.23	--	--	--	--	--	--	--	--
V	µg/L	0.1	MS	< 0.1	< 0.1	< 0.1	< 0.1	< 0.1	< 0.1	< 0.1	< 0.1	< 0.1
W	µg/L	0.02	MS	0.12	0.07	0.12	0.04	< 0.02	0.03	0.03	0.08	0.05
Y	µg/L	0.003	MS	1.51	1.02	0.44	2.76	0.05	0.117	0.041	0.054	0.019
Yb	µg/L	0.001	MS	0.035	0.01	0.006	0.024	0.005	0.008	0.002	0.003	0.002
Zn	µg/L	0.5	MS	> 250	> 250	> 250	> 250	> 250	> 250	231	> 250	> 250
Zn	µg/L	5	OES	2350	1610	969	712	496	386	--	323	460
Zr	µg/L	0.01	MS	0.13	0.14	0.03	0.03	0.38	0.24	0.06	0.07	0.07

Mineralogical sources of leachate target analytes

The rock characterization study demonstrates the chemical variability of the starting materials and the mineralogical source of leaching analytes. Some target analytes are present in several minerals that have different weathering characteristics; others are largely confined to a few mineral groups. Based on the data presented in this chapter, the main sources for the target analytes are as follows:

- Aluminum: Micas (muscovite, biotite, phengite), clay (illite, kaolin), chlorite, feldspar
- Calcium: Calcite, ankerite, apatite
- Iron: Pyrite, ankerite, siderite, micas, chlorite
- Manganese: Ankerite, calcite, siderite, pyrite, chlorite, biotite
- Potassium: Micas, feldspar
- Magnesium: Ankerite, chlorite, micas
- Selenium: Pyrite, organic material(?)
- Zinc: Sphalerite
- Sulfur (sulfate): Pyrite, gypsum, barite

Iron is not likely to be a good indicator of pyrite weathering progress because of the variable iron content of the carbonate minerals. Both pyrite and carbonates contribute iron to the leachates. During rock weathering, the best predictor of potential acid production is the carbonate content (Perry, 1998; Brady et al., 2004; Jambor et al., 2005). Once the available carbonate in the rock is exhausted or unavailable for NP generation due to inhibition by armoring, then the "runaway" acid-generation condition can develop. The nature of the carbonate mineral is important because not all carbonates produce alkalinity. It is well-known that siderite, for example, overestimates alkalinity determined by acid-base accounting because the ferrous iron released from the dissolving carbonate is oxidized to ferric iron which undergoes hydrolysis and precipitation (Skousen et al., 1997). Differences in carbonate mineral composition among samples, as well as carbonate mineral abundances and textures, will affect the weathering behavior of these rocks. Pyrite is present as framboids in all of the samples. The framboids form clusters of extremely fine-grained individual crystals with lots of surface area, and therefore are likely to be highly reactive. Some pyrite is in contact with calcite which provides inherent NP. Although apatite is a minor component of these rocks, it occurs in contact with pyrite in some places, and provided NP. Manganese is present in pyrite as well as in carbonate minerals.

The major minerals present in the shales are quartz, muscovite/illite, chlorite; the amounts of pyrite and carbonate minerals vary. XRD patterns for the raw shale samples are shown in Figure 5.39, along with the reference patterns for quartz, pyrite, chlorite, and muscovite. Relative amounts of different minerals, and relative amounts of different carbonate minerals, in each sample are plotted as bar charts in Figure 5.40. Accessory minerals include apatite, zircon, and rutile. Siderite and ankerite are less soluble than calcite. Furthermore, the zoning of some carbonates suggests that leachate chemistry could change as weathering proceeds and carbonate is consumed. In addition to carbonate minerals and apatite, some silicate minerals provide long-term NP that may be a factor in natural weathering, but probably does not occur on the time scales of the leaching tests. The silicate minerals in the shales that may contribute NP

are chlorite and biotite. Although calcic feldspars are known to contribute NP, the feldspars identified in these rocks are mainly sodic. Quartz is inert. Jambor et al's (2002) static NP

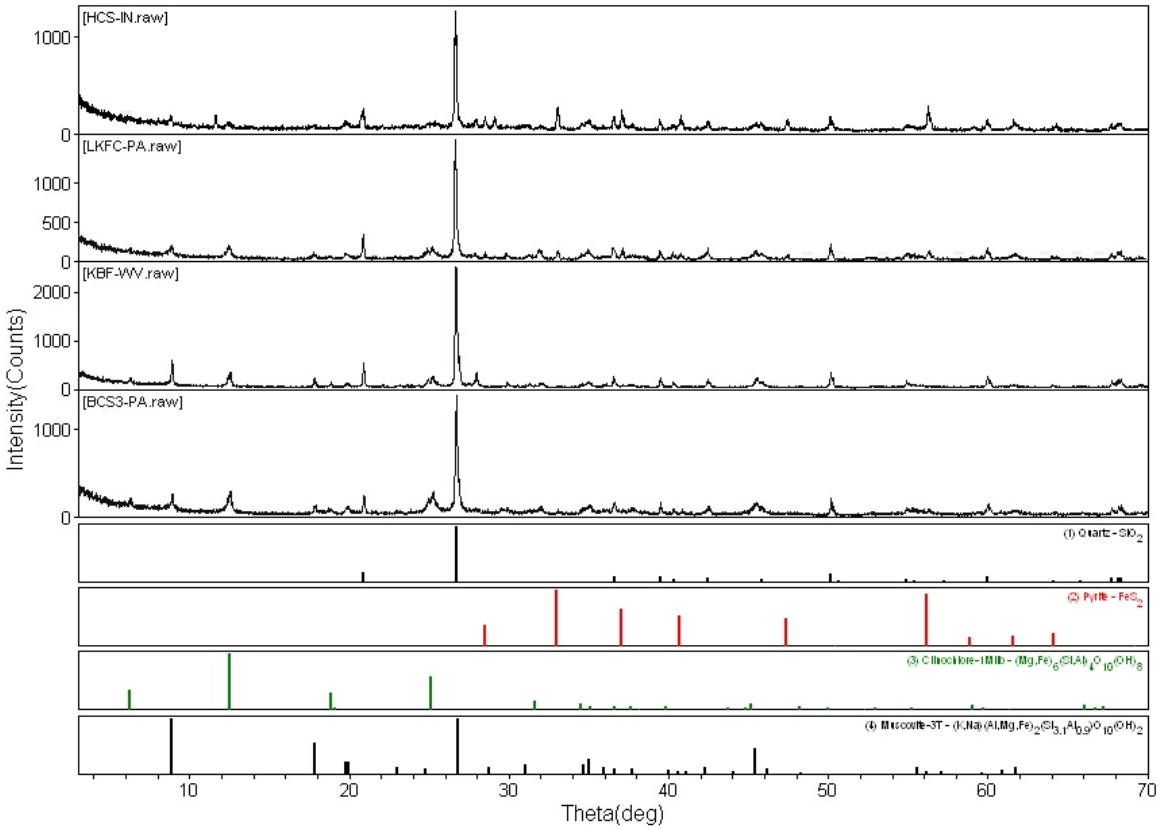

Figure 5.39. XRD patterns for shales and peak locations for standard reference patterns for quartz, pyrite, chlorite (clinochlore variety), and muscovite. Note that the strongest peak in each XRD pattern is the most intense quartz peak at 26.6 degrees.

determinations on individual minerals show that most rock-forming silicate and aluminosilicate minerals provide insufficient NP to produce a threshold NP of 20 kg $CaCO_3$ equivalent. Ideal formulas for minerals identified in the ADTI samples are listed in Table 5.3, along with comments on weathering behavior (based on Goldrich, 1938) and potential acid-neutralizing capacity of individual minerals based on relative reactivities of monomineralic samples at pH5 (Sverdrup, 1990) and NP determinations for monomineralic samples (Jambor et al., 2002). Relative dissolution rates for calcite in laboratory experiments at pH5 are several orders of magnitude faster than dissolution rates for any of the silicate minerals such as biotite or chlorite (Jambor, 2003; Kowalewski and Rimstidt, 2003). Textural relations, such as pyrite in contact with calcite as shown in Figure 5.13, demonstrate inherent neutralization for oxidative weathering of pyrite. Although none of the leach effluents in the USGS experiments were net acidic after the 16 weeks of the experiment, the relative rates of exhaustion of pyrite versus calcite determine long-term weathering behavior of the samples. Leachate experiments on Houchin Creek Shale from some of the other laboratories did go acidic during the final weeks of the experiments. See Chapter 8 for evaluation of weathering rates and predictions of the long-term weathering behavior of the samples based on the complete interlaboratory data set.

Low-temperature ash determinations as well as optical and scanning-electron microscopy show that organic material is a significant component of the Houchin Creek Shale and the Leechburg Coal Refuse. Minor amounts of organic material are observed in other samples. The

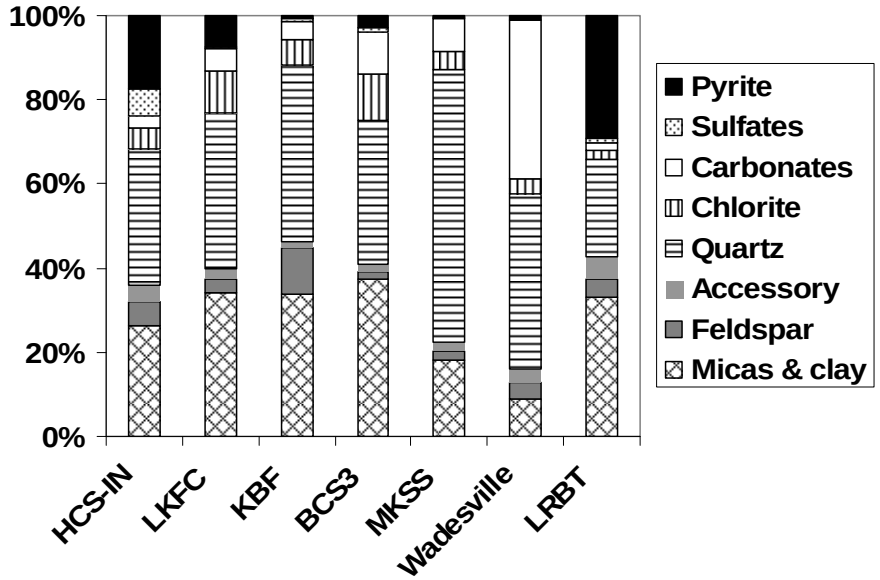

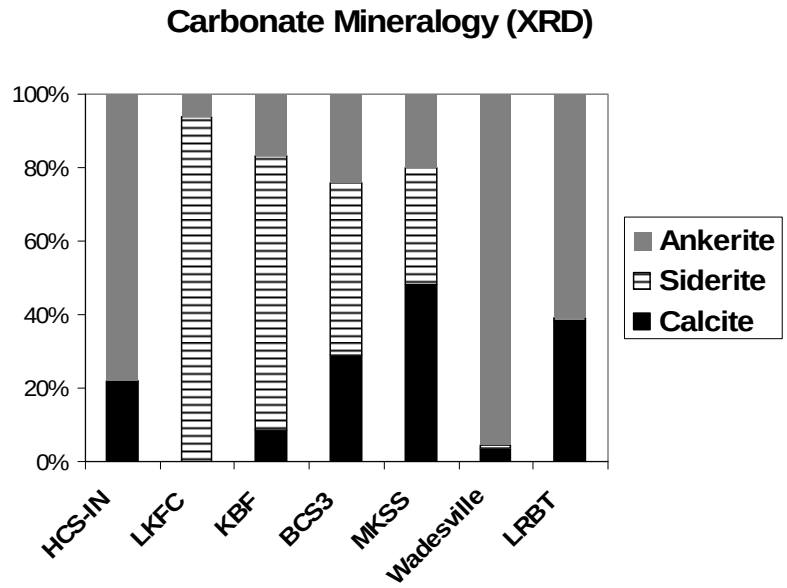

Figure 5.40. Bar charts showing relative percentages of different minerals in the crystalline parts of the samples based on quantitative x-ray powder diffraction (XRD). The bottom chart shows the relative percentages of different carbonate minerals. For example, the Houchin Creek Shale (HCS-IN) has only 3 weight percent total carbonate minerals. The carbonate mineral makeup of that 3 weight per cent is: 0% siderite, 78% ankerite, and 22% calcite.

presence of organic material may affect the production and (or) transport of carbon dioxide in leaching columns. The organic matter could decompose generating carbon dioxide, or it could sorb carbon dioxide generated by acid reaction with carbonate minerals or introduced with compressed air.

Mineralogical Controls on Leachate Quality

Differences in mineralogy among the five lithologies tested are reflected in leach column effluents. We examined mineralogical controls on leachate quality by comparing the cumulative sulfate–sulfur, calcium, and alkalinity leached from the samples during the 16 weeks of the experiment with bulk rock total sulfur, total calcium (as CaO), and estimated abundances of pyrite and carbonate minerals in starting materials. We also computed the percentage of initial sulfur leached during the course of the experiment. These calculations are based on total sulfur in the rock (Table 5.2) and leach column effluent data from the USGS laboratory; data and calculations are given in Appendix 5.2.

The cumulative amount of sulfate leached from the rocks at the end of 16 weeks is consistent with the relative abundance of pyrite (and total sulfur) in the starting material, but does not correlate directly with initial sulfur concentrations measured by TD-ICP (Figure 5-41*A)*. The Houchin Creek Shale contains an estimated 17 weight percent pyrite[2] (4.33 weight percent initial sulfur). The Middle Kittanning Sandstone contains 0.4 weight percent pyrite (<0.1 weight percent total initial sulfur). Less than 10 percent of the initial sulfur present in any of the samples was leached during the experiment (Figure 41*B*). Although the Lower Kittanning Shale contains much less pyrite (8 weight percent) and total sulfur (<1 weight percent) than the Houchin Creek Shale, the percentage of total sulfur leached from the Lower Kittanning sample after 16 weeks was three times as great. The Houchin Creek Shale is a finer-grained rock than the Lower Kittanning Shale. The Houchin Creek Shale contains a significant amount of organic material; carbonate minerals include calcite and ankerite. The Lower Kittanning Shale contains very little organic material, the dominant carbonate mineral is siderite, and both coarse and framboidal pyrite are observed. These differences may affect the kinetics of pyrite weathering in the two shales.

The cumulative alkalinity in leach column effluent and the initial carbonate mineral content of the starting materials are not closely related (Figure 5.42). Although the Brush Creek Shale, with an estimated 10 weight percent total carbonate minerals, generated the highest cumulative alkalinity, the Kanawha Black Flint Shale, with only 4 weight percent total carbonate minerals generated greater cumulative alkalinity than the Middle Kittanning Sandstone, with 8 weight percent total carbonates. The Brush Creek Shale and the Houchin Creek Shale both contain 2.25 weight percent CaO (Table 5.2), yet they the generated different amounts of alkalinity during the course of the experiment. The Brush Creek and Houchin Creek shales contain an estimated 2.9 and 0.6 weight percent calcite, respectively. The Brush Creek shale contains siderite as well as calcite (Ca-rich cores and Fe-rich rims). No siderite was observed in Houchin Creek Shale. Although it contained 5 weight percent total carbonates, the Lower Kittanning Shale generated the least alkalinity during the weathering experiment (Figure 5.42). Siderite is the dominant carbonate minerals in the Lower Kittanning Shale; calcite was only observed within a fossil-rich clast. The presence of calcite appears to exert a strong control on alkalinity in column effluent. Although the quantitative XRD data are uncertain for low concentrations of minerals in complex

[2] Mineral percentages based on crystalline component

rocks such as these, the data suggest that the nature of the carbonate mineral as well as the amount of carbonate minerals affects leachate quality. The occurrence of a variety of different carbonate minerals, including siderite and zoned carbonate minerals, may explain some of the complications associated with NP determinations in acid-base accounting that lead to uncertainties in mine drainage prediction.

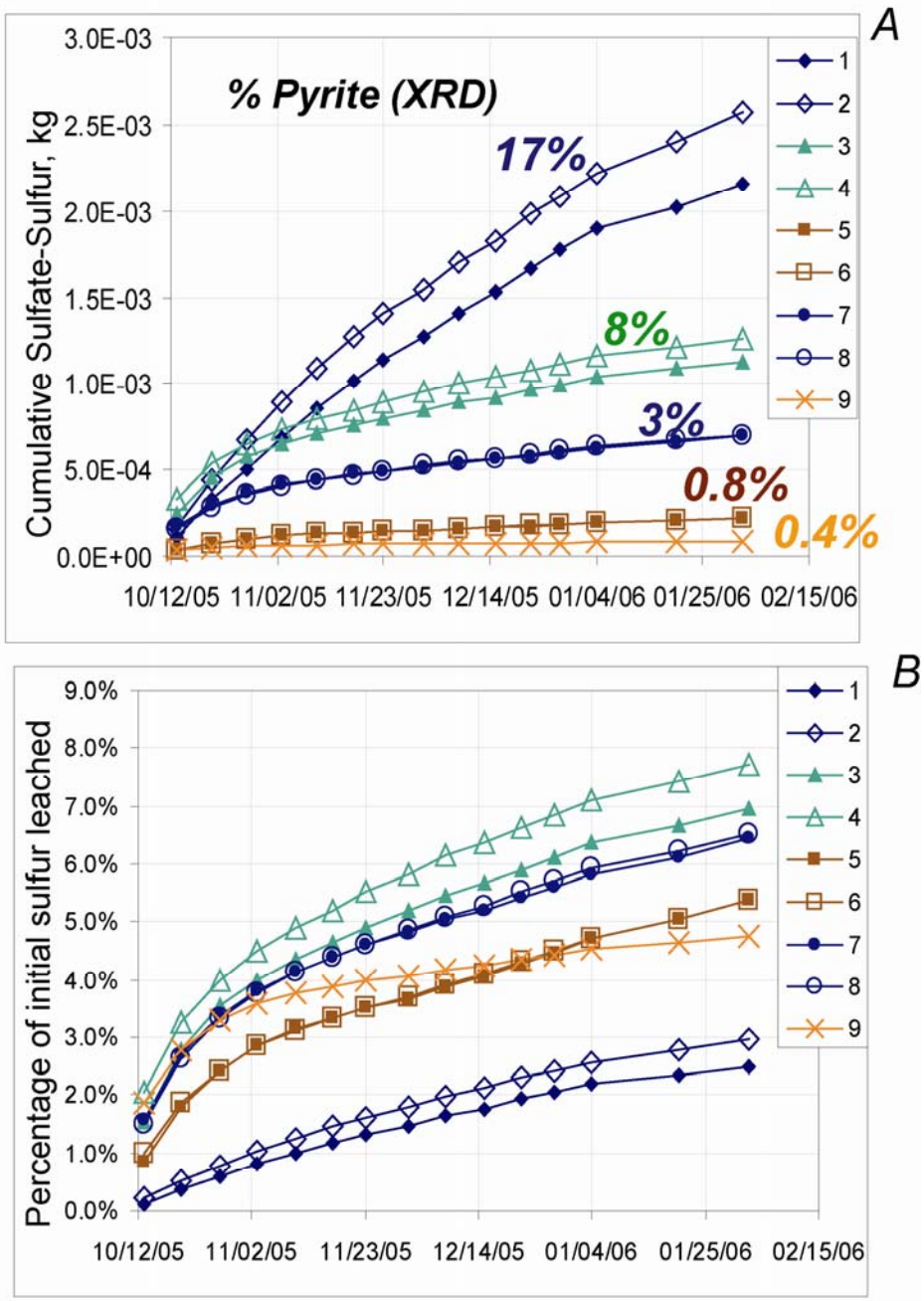

Figure 5.41. Sulfur in leach column effluent as a function of time for duplicate columns of Houchin Creek Shale (1 and 2), Lower Kittanning Shale (3 and 4), Kanawha Black Flint Shale (5 and 6), Brush Creek Shale (7 and 8), and a single column of Middle Kittanning Sandstone (9). *A*, Cumulative sulfate-sulfur. Curves are labeled with the weight percent pyrite determined by XRD (Table 5.4). *B*, Percentage of initial sulfur leached. Initial sulfur based on chemical analyses by TD-ICP reported in Table5.2. See Appendix 5.2 for leachate data and calculations.

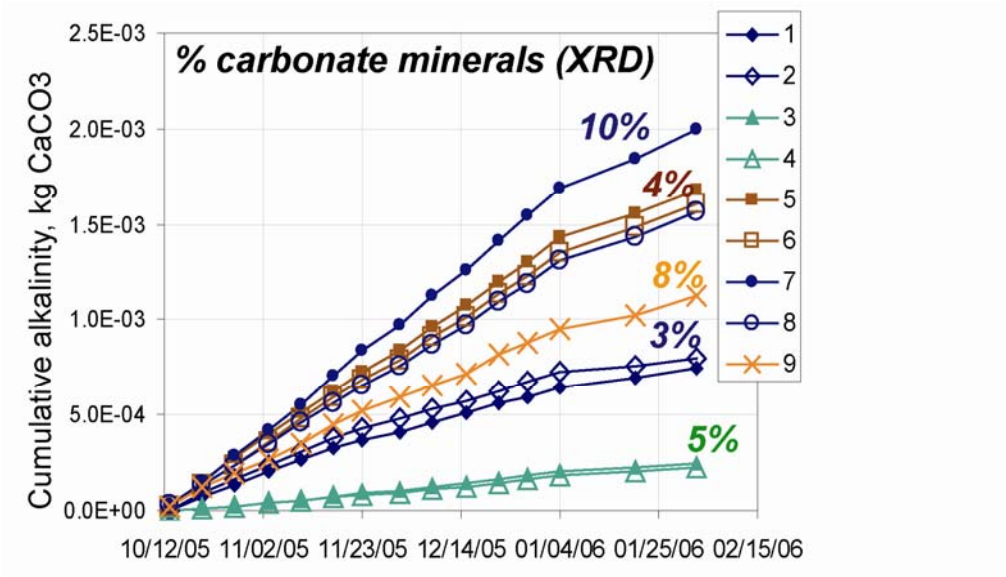

Figure 5.42. Cumulative alkalinity in column effluent as a function of time for duplicate columns of Houchin Creek Shale (1 and 2), Lower Kittanning Shale (3 and 4), Kanawha Black Flint Shale (5 and 6), Brush Creek Shale (7 and 8), and a single column of Middle Kittanning Sandstone (9). Curves are labeled with the weight percent total carbonate minerals determined by XRD (Table 5.4). See Appendix 5.2 for data and calculations.

Literature Cited

Ball, J.W., and D.K., Nordstrom. 1991. User's manual for WATEQ4F with revised data base: U.S. Geological Survey Open-File Report 910183, 189 p.

Brady, K.B.C., Hornberger, R.J., and G. Fleeger. 1998. Influence of geology on post-mining water quality: Northern Appalachian Basin. Chapter 8. *In* Coal Mine Drainage Prediction and Pollution Prevention in Pennsylvania, Harrisburg. Pennsylvania Dept. of Environmental Protection.

Brady, K.B.C., White, W.B., Hornberger, R.J., Scheetz, B.E., and C.M. Loop. 2004. Refinement of ADTI-WP2 standard weathering procedures, and evaluation of particle size and surface area effects upon leaching rates: Part 2: Practical and theoretical aspects of leaching kinetics. 2004 National Meeting of the American Society of Mining and Reclamation and the 25th West Virginia Surface Mine Drainage Task Force, April 18-24, 2004. Published by ASMR, 3134 Montavesta Rd., Lexington, KY 40502. p. 174-200.

Chang, L.L.Y., Howie, R.A., and J. Zussman. 1996. Rock-forming Minerals, Deer, Howie and Zussman Volume 5B, Non-silicates: Sulphates, Carbonates, Phosphates, Halides, 2nd ed., Longman Group, Ltd., Essex, England.

Goldrich, S.S. 1938, A study in rock-weathering. Journal of Geology v. 46, p. 17-58.

Hem, J.D. 1985. Study and interpretation of the chemical characteristics of natural waters (3rd): U.S. Geological Survey Water-Supply Paper 2254, 263 p.

Hornberger, R.J. and K.B.C. Brady. 1998. Kinetic (leaching) tests for the prediction of mine drainage quality. In: Coal Mine Drainage Prediction and Pollution prevention in Pennsylvania, Harrisburg: Pennsylvania Department of Environmental Protection, pp. 7 - 1 to 7 - 54.

Hornberger, R.J., Brady, K.B.C., Cuddeback, J.E., Telliard, W.A., Parsons, S.C., Scheetz, B.E., and T.W. Bergstresser. 2003. Development of the ADTI-WP1 (humidity cell) and ADTI-WP2 (leaching column) standard weathering procedures for coal mine drainage prediction. *In* Proceedings from the Fifth International Conference on Acid Rock Drainage, Littleton, CO. Society for Mining Metallurgy and Exploration, p. 41-50.

Hornberger, R.J., Brady, K.B.C., Cuddeback, J.E., White, W.B., Scheetz, B.E., Telliard, W.A., Parsons, S.C., Loop, C.M., Bergstrasser, T.W., McCracken, C.R., Jr., and D. Wood. 2004. Refinement of ADTI-WP2 standard weathering procedures, and evaluation of particle size and surface area effects upon leaching rates: Part 1: Laboratory evaluation of method performance. 2004 National Meeting of the American Society of Mining and Reclamation and the 25th West Virginia Surface Mine Drainage Task Force, April 18-24, 2004. Published by ASMR, 3134 Montavesta Rd., Lexington, KY 40502. p. 916-945.

Hornberger, R.J., Brady, K.B.C., Scheetz, B.E., White, W.B., and S.C. Parsons. 2005. ADTI-WP2 leaching column method for overburden analysis and prediction of weathering rates. In: Proceedings of 26th West Virginia Surface Mine Drainage Task Force Symposium, Morgantown, West Virginia, p. 93-110.

ICDD. 2002. Powder Diffraction File release 2002, PDF-2: International Centre for Diffraction Data, Newton Square, PA.

Jambor, J.L. 2003. Mine-waste mineralogy and mineralogical perspectives of acid-base accounting. *In* Jambor, J.L., Blowes, D.W., and A.I.M. Ritchie (eds), Environmental aspects of mine wastes, Mineralogical Association of Canada, Short Course Series, Volume 31, p. 117-145.

Jambor, J.L., Dutrizac, J.E., Groat, L.A., and M. Raudsepp. 2002. Static tests of neutralization potentials of silicate and aluminosilicate rocks. Environmental Geology 43: 1-17.

Jambor, J.L., Dutrizac, J.E., and M. Raudsepp. 2005. Comparison of measured and mineralogically predicted values of the Sobek neutralization potential for intrusive rocks. In 7th International Conference on Acid Rock Drainage (ICARD), March 26-30, 2006, St. Louis, MO. R.I. Barnhisel (ed). Published by the American Society for Mining and Reclamation, Lexington, KY, p. 820-832.

Kowalewski, M. and J.D. Rimstidt. 2003. Average lifetime and age spectra of detrital grains: Toward a unifying theory of sedimentary particles. Journal of Geology 111: 427-439.

Langmuir, D.1997. Aqueous environmental geochemistry: New Jersey, Prentice-Hall, 600 p.

Mitchell, R.S. and H.J. Gluskoter. 1976. Mineralogy of ash of some American coals: variations with temperature and source. Fuel Lond. 55, 90-96.

Pearson, D.E. and J. Kwong. 1979. Mineral matter as a measure of oxidation of a coaking coal. Fuel, London, 58: 63-66.

Perry, E.F. 1998. Interpretation of acid-base accounting. Chapter 11. *In* Coal Mine Drainage Prediction and Pollution Prevention in Pennsylvania, Harrisburg. Pennsylvania Dept. of Environmental Protection.

Pontolillo, J. and R.W. Stanton. 1994. Coal Petrographic Laboratory Procedures and Safety Manual II. U.S. Geological Survey Open-File Report 94-631.

Rao, C. P. and H.J. Gluskoter. 1973. Occurrence and Distribution of Minerals in Illinois Coals, Circular 476, Illinois State Geological Survey, Urbana, 56 p.

Raudsepp, M. and E. Pani. 2003. Application of Rietveld analysis to environmental mineralogy. *In* Jambor, J.L., Blowes, D.W., and A.I.M. Ritchie (eds), Environmental aspects of mine wastes, Mineralogical Association of Canada, Short Course Series, Volume 31, p. 165-180.

Skousen, J., Renton, J., Brown, H., Evans, P., Leavitt, B., Brady, K., Cohen, L., and P. Ziemkiewicz. 1997. Neutralization potential of overburden samples containing siderite. J. Environmental Quality 26, p. 673-681.

Snoeyink, V.L., and D. Jenkins, D. 1980. Water chemistry: New York, John-Wiley & Sons, p. 289-292.

Sverdrup, H.U. 1990. The kinetics of base cation release due to chemical weathering. Lund University Press, Lund, Sweden, 246 p.

Taylor, J.C., and R.A. Clapp.1992. New features and advanced applications of Siroquant: A personal computer XRD full profile quantitative analysis software package: Advances in X-ray Analysis, v. 35, p. 49-55.